Biomedicine & Pharmacotherapy 179 (2024) 117313

Contents lists available at ScienceDirect

Biomedicine & Pharmacotherapy

journal homepage: www.elsevier.com/locate/biopha

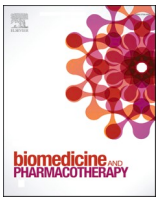

The autophagy-targeting compound V46 enhances antimicrobial responses to *Mycobacteroides abscessus* by activating transcription factor EB

Asmita Sapkota [a,1], Eun-Jin Park [a,b,c,d,1], Young Jae Kim [a,b,c,d,1], Jong Beom Heo [b,e,1], Thanh Quang Nguyen [f], Bo Eun Heo [f], Jin Kyung Kim [g], Sang-Hee Lee [h], Soo In Kim [a,b,c,d], Yoon-Jung Choi [b,e], Taylor Roh [a,b,c,d], Sang Min Jeon [a,b,c,d], Marnpyung Jang [i], Hae Joon Heo [b,e], Jake Whang [j], Seungwha Paik [a,d], Jae-Min Yuk [b,d,k], Jin-Man Kim [b,d,l], Gyu Yong Song [b,e,*], Jichan Jang [f,**], Eun-Kyeong Jo [a,b,c,d,***]

[a] *Department of Microbiology, College of Medicine, Chungnam National University, Daejeon, South Korea*
[b] *Infection Control Convergence Research Center, College of Medicine, Chungnam National University, Daejeon, South Korea*
[c] *Brain Korea 21 FOUR Project for Medical Science, College of Medicine, Chungnam National University, Daejeon, South Korea*
[d] *Department of Medical Science, College of Medicine, Chungnam National University, Daejeon, South Korea*
[e] *College of Pharmacy, Chungnam National University, Daejeon, South Korea*
[f] *Division of Life Science, Department of Bio & Medical Big Data (BK21 Four Program), Research Institute of Life Science, Gyeongsang National University, Jinju, South Korea*
[g] *Department of Microbiology, Keimyung University, School of Medicine, Daegu, South Korea*
[h] *Center for Research Equipment, Korea Basic Science Institute, Cheongju, Chungbuk, South Korea*
[i] *College of Medicine, Chungnam National University, Daejeon, South Korea*
[j] *Korea Mycobacterium Resource Center & Basic Research Section, The Korean Institute of Tuberculosis, Cheongju, South Korea*
[k] *Department of Infection Biology, College of Medicine, Chungnam National University, Daejeon, South Korea*
[l] *Department of Pathology, College of Medicine, Chungnam National University, Daejeon, South Korea*

Abbreviations: AMK, amikacin; AMP, adenosine monophosphate; AMPK, adenosine monophosphate-activated protein kinase; ANOVA, analysis of variance; Baf-A1, bafilomycin A1; BDQ, bedaquiline; BMDM, bone marrow-derived macrophage; CCK-8, cell counting kit-8; CFU, colony forming unit; CFX, cefoxitin; CKO, conditional knockout; CLA, clarithromycin; Com., compound; CQ, chloroquine diphosphate salt; DAPI, 4',6-diamidino-2-phenylindole; Der., derivative; DMEM, Dulbecco's Modified Eagle Medium; DMF, dimethylformamide; Dpi, days post-infection; EGFP, enhanced green fluorescent protein; ELISA, enzyme linked immunosorbent assay; ERK1/2, extracellular signal receptor kinase 1/2; FBS, fetal bovine serum; FIC, fractional inhibitory concentrations; GFP, green fluorescent protein; H&E, hematoxylin and eosin; HMDM, human monocyte-derived macrophage; IL, interleukin; IMP, imipenem; JNK, c-Jun N-terminal kinase; KO, knockout; LAMP1, Lysosomal-associated membrane protein 1; LC3, microtubule-associated protein 1 light chain 3; Mabc, *Mycobacteroides abscessus* complex *abscessus*; Mabc-S, *Mycobacteroides abscessus* complex *abscessus* smooth type variants; Mabc-R, *Mycobacteroides abscessus* complex *abscessus* rough type variants; MAPK, mitogen-activated protein kinase; Mboll, *Mycobacteroides abscessus* complex *bolletii*; MDR, multidrug-resistant; MDR-Mabc, multidrug-resistant strain of Mabc; MIC, minimal inhibitory concentration; MIC_{50}, MIC required to suppress bacterial growth by 50 %; MOI, multiplicity of infection; Mtb, *Mycobacterium tuberculosis*; mTOR, mammalian target of rapamycin; NF-κB, nuclear factor kappa B; NMR, nuclear magnetic resonance; n.s., not significant; NTM, nontuberculous mycobacteria; OADC, oleic albumin dextrose catalase; OD, optical density; OMD, omadacycline; PBMC, peripheral blood mononuclear cell; PBS, phosphate buffered saline; PBST, phosphate buffered saline with 0.05 % Tween 80; P, phospho; qRT-PCR, quantitative real-time PCR; REMA, resazurin reduction microplate assay; RFB, rifabutin; ROS, reactive oxygen species; RSV, resveratrol; RT, room temperature; SC, solvent control; SD, standard deviation; SEM, standard error of the mean; SIRT, Sirtuin; STAT3, signal transducer and activator of transcription 3; TEM, transmission electron microscopy; TFEB, transcription factor EB; TLC, thin layer chromatography; V46, *trans*-3,5,4′-trimethoxystilbene; WT, wild-type; ZF, zebrafish.

* Corresponding author at: College of Pharmacy, Chungnam National University, Daejeon, South Korea.
** Corresponding author at: Division of Life Science, Department of Bio & Medical Big Data (BK21 Four Program), Research Institute of Life Science, Gyeongsang National University, Jinju, South Korea.
*** Corresponding author at: Department of Microbiology, College of Medicine, Chungnam National University, Daejeon, South Korea.
E-mail addresses: gysong@cnu.ac.kr (G.Y. Song), jichanjang@gnu.ac.kr (J. Jang), hayoungj@cnu.ac.kr (E.-K. Jo).
[1] These authors contributed equally to this work and share first authorship.

https://doi.org/10.1016/j.biopha.2024.117313
Received 21 February 2024; Received in revised form 12 August 2024; Accepted 13 August 2024
Available online 20 August 2024

ARTICLE INFO

Keywords:
V46
Mycobacteroides abscessus
Transcription factor EB
Inflammation
Host defense
Autophagy

ABSTRACT

Mycobacteroides abscessus (Mabc) is a rapidly growing nontuberculous mycobacterium that poses a considerable challenge as a multidrug-resistant pathogen causing chronic human infection. Effective therapeutics that enhance protective immune responses to Mabc are urgently needed. This study introduces *trans*-3,5,4′-trimethoxystilbene (V46), a novel resveratrol analogue with autophagy-activating properties and antimicrobial activity against Mabc infection, including multidrug-resistant strains. Among the resveratrol analogues tested, V46 significantly inhibited the growth of both rough and smooth Mabc strains, including multidrug-resistant strains, in macrophages and in the lungs of mice infected with Mabc. Additionally, V46 substantially reduced Mabc-induced levels of pro-inflammatory cytokines and chemokines in both macrophages and during *in vivo* infection. Mechanistic analysis showed that V46 suppressed the activation of the protein kinase B/Akt-mammalian target of rapamycin signaling pathway and enhanced adenosine monophosphate-activated protein kinase signaling in Mabc-infected cells. Notably, V46 activated autophagy and the nuclear translocation of transcription factor EB, which is crucial for antimicrobial host defenses against Mabc. Furthermore, V46 upregulated genes associated with autophagy and lysosomal biogenesis in Mabc-infected bone marrow-derived macrophages. The combination of V46 and rifabutin exerted a synergistic antimicrobial effect. These findings identify V46 as a candidate host-directed therapeutic for Mabc infection that activates autophagy and lysosomal function via transcription factor EB.

1. Introduction

Nontuberculous mycobacteria (NTM), which cause severe pulmonary and ulcerative infections, are becoming increasingly prevalent worldwide [1,2]. Although formerly considered opportunistic in immunocompromised individuals, NTM infections frequently occur in immunocompetent hosts [3,4]. Among NTM, the *Mycobacteroides abscessus* complex, comprising *M. abscessus* (Mabc), *M. massiliense*, and *M. bolletii* (Mboll) [5], is notable for its rapid growth and carriage of an inducible macrolide resistance gene [*erm* [41]], enabling it to cause clinically severe infection [6]. The resolution of Mabc infection is hampered by its intrinsic resistance to multiple antibiotics, emphasizing the need for a greater understanding of host immune responses to develop effective therapeutics [7–9]. However, the current understanding of host protective immune responses is inadequate for this purpose.

Autophagy, a cell-autonomous catabolic pathway, is crucial for host defenses against intracellular infections by mycobacteria, including NTM [10,11]. Although the role of autophagy in *Mycobacterium tuberculosis* (Mtb) infection has been extensively investigated, its role in NTM infections is less understood [12]. Prolonged azithromycin administration to cystic fibrosis patients impairs autophagic degradation of mycobacteria, increasing susceptibility to NTM infection [13]. Enhanced lysosomal activity and phagosomal maturation have been linked to improved host defenses against Mabc infection [14,15]. Transcription factor EB (TFEB) is critical for autophagy and lysosomal biogenesis, thereby enhancing antimicrobial defenses against intracellular bacterial infections [16–18]. Recent research has identified promising candidate drugs that suppress Mabc replication within macrophages, activate multiple immune pathways, and demonstrate therapeutic efficacy *in vivo* [14,15,19]. Despite these advances, there are few drug candidates specifically targeting autophagy and TFEB to enhance innate immune defenses against Mabc infection. Such efforts could pave the way for developing new host-directed therapies to combat Mabc infections, which are frequently complicated by drug resistance.

Resveratrol (RSV) is a phytoalexin of the stilbene family and a common compound in plants; it is synthesized via the phenylpropanoid pathway in response to various stressors, infections, injuries, ultraviolet radiation, and fungicides [20,21]. RSV exhibits the pharmacological characteristics of stilbene compounds, including antioxidant, anti-inflammatory, and immunomodulatory effects [22,23]. However, its rapid metabolism and low bioavailability hinder its therapeutic use [24]. To overcome these limitations, we synthesized multiple RSV analogues. Among them, *trans*-3,5,4′-trimethoxystilbene (V46) exhibited potent antimicrobial activity against both Mabc rough (Mabc-R) and smooth (Mabc-S) variants, including multidrug-resistant (MDR) strains, in macrophages and *in vivo*. The immunomodulatory function of V46 in antimicrobial responses to Mabc infection was found to be autophagy- and TFEB-dependent. When combined with rifabutin (RFB), V46 demonstrated synergistic antimicrobial activity, highlighting its potential as a therapeutic agent for Mabc infection.

2. Materials and methods

2.1. Mice

Female wild-type (WT) C57BL/6 mice aged 7–8 weeks were obtained from Samtako Bio (Gyeonggi-do, South Korea), and female WT C3HeB/FeJ mice aged 8 weeks were acquired from The Jackson Laboratory (Bar Harbor, ME, USA). *Atg7*-floxed mice ($Atg7^{fl/fl}$) derived from C57BL/6 mice were kindly provided by Prof. Masaaki Komatsu (Tokyo Metropolitan Institute of Medical Science, Tokyo, Japan). Myeloid cell-specific *Atg7*-deficient (*Atg7* conditional knockout (cKO); $Atg7^{-/-}$) mice and their littermates (*Atg7* WT; $Atg7^{+/+}$) were generated using the LysM-Cre system as previously described [25]. Sirtuin 1 (*Sirt1)* WT and KO mice were kindly provided by Prof. Byung-Hyun Park (Department of Biochemistry, Chonbuk National University Medical School, South Korea). *Sirt3* WT and KO mice were kindly provided by Prof. Hyun Seok Kim (Ehwa Woman's University, Seoul, South Korea). Mice (sex-matched; 7–8 weeks old) were maintained under a 12:12 h light:dark cycle and specific-pathogen-free conditions. Animal experiments were performed in accordance with the applicable ethical guidelines.

2.2. Mycobacterial strains and cultivation

2.2.1. Preparation of Mabc strains and inocula

Mabc-S ATCC19977 or CIP104536^T and isogenic Mabc-R were used in this study. Strain ATCC19977 was obtained from the American Type Culture Collection, and CIP104536^T was kindly provided by Dr. Laurent Kremer (CNRS, IRIM, Universite' de Montpellier, Montpellier, France). The genetically identical Mabc-R strain was obtained by continuous anaerobic passaging of ATCC19977 or CIP104536^T. For confocal analysis and three-dimensional holographic imaging, an Mabc (CIP104536^T) strain harboring pMV262-mWasabi [hereafter green fluorescent protein (GFP)-Mabc] was constructed as previously described [19]. Mboll (KMRC-00800–00023) and the MDR strains of Mabc (KMRC-00800–00010 and −00011; KMRC-010 and KMRC-011, respectively) were acquired from the Korean Mycobacterium Resource Center. The MDR-Mabc strains were resistant to rifampicin, ethambutol, and clarithromycin (CLA). Mabc and Mboll strains were cultured in Middlebrook 7H9 (Difco, 271310) medium supplemented with 10 % oleic albumin dextrose catalase (OADC) (BD Biosciences, San Diego, CA, USA), 0.5 % glycerol (Sigma-Aldrich, St. Louis, MO, USA), and

0.05 % Tween-80 (Sigma-Aldrich) on a rotary shaking incubator (140 rpm) at 37℃ to an optical density (OD)600 of 0.4–0.6. For strains expressing fluorescent proteins, 50 μg/mL kanamycin was added to cultures. Harvested culture pellets were prepared to generate single-cell suspensions as previously described [26]. Representative vials were thawed, and colony-forming units (CFUs) were counted on Middlebrook 7H10 agar (Difco, 262710).

2.2.2. Preparation of Mabc strains and inocula for zebrafish (ZF) infection

GFP-Mabc was cultured in Middlebrook 7H9 broth with albumin dextrose saline and 0.05 % Tween 80 (Sigma-Aldrich) at 30℃ for 7 days [19]. Mid-log phase cultures were harvested, cleaned, and resuspended in phosphate-buffered saline (PBS) supplemented with 0.05 % Tween-80 (PBST). The resulting bacterial inoculum was homogenized by passaging with a 26-gauge needle and sonication in a water bath at 40 kHz, three times for 30 s each (Branson CPX3800, Danbury, CT, USA). Aliquots (5 μL) of bacterial stocks were stored at −80℃. Before injection, CFUs were enumerated on 7H10 agar. The inoculum for infection comprised 130 CFUs/mL in PBST and 0.085 % phenol red [27].

2.3. Isolation of bone marrow-derived macrophages (BMDMs)

BMDMs were isolated as previously described [26]. Briefly, BMDMs were extracted from the femurs and tibiae of 7–8-week-old female C57BL/6 mice. Bone marrow cells were cultured for 4–5 days in Dulbecco's modified Eagle's medium (DMEM; Lonza, Walkersville, MD, USA, BE12–60F) containing 10 % fetal bovine serum (FBS; Gibco, Grand Island, NY, USA), 1 % penicillin-streptomycin (Lonza, 17–745E), and macrophage colony-stimulating factor (25 ng/mL; R&D Systems, Minneapolis, MN, USA) at 37℃ in a 5 % CO_2 atmosphere. After differentiation, cells were maintained in fresh medium containing only 5 % FBS.

2.4. Isolation of human monocyte-derived macrophages (hMDMs)

Human peripheral blood mononuclear cells (PBMCs) were isolated from heparinized venous blood of healthy volunteers by Ficoll-Hypaque gradient centrifugation (Lymphoprep; Axis-Shield, Dundee, UK, 1114544). To differentiate macrophages from PBMCs, adherent monocytes were cultured in Roswell Park Memorial Institute 1640 medium (Lonza, Basel, Switzerland, 12–702 F) supplemented with 10 % pooled human serum (Sigma-Aldrich, H4522) and 1 % L-glutamine, 50 μg/mL streptomycin, and 50 IU/mL penicillin (Lonza, 17–745E) for 1 h at 37℃. Nonadherent cells were discarded. hMDMs were prepared by culturing PBMCs for 4 days with 4 ng/mL human macrophage colony-stimulating factor (Sigma-Aldrich, M6518). These procedures were approved by the Institutional Research and Ethics Committee of Chungnam National University.

2.5. Experimental infection

After thawing from −80℃, bacteria were diluted in Dulbecco's PBS (SH30028.02; Cytiva HyClone™, Marlborough, MA, USA) containing 0.05 % Tween-80, then sonicated in a water bath three times for 30 s each. BMDMs were infected with Mabc or Mboll at the indicated multiplicities of infection (MOIs) for 2 h and incubated in fresh DMEM (Lonza) for the indicated times. For *in vivo* infection, mice were anesthetized using avertin (2,2,2-tribromoethanol dissolved in 2-mercaptoethanol) and intranasally infected with Mabc, including MDR strains (1×10^6, 1×10^5, or 1×10^3 CFUs/mouse) for 5, 10, or 21 days, respectively. Most experiments were conducted using the Mabc-R strain (labeled "Mabc"), with the exception of intracellular survival assays and resazurin microtiter assays (REMA), which used the Mabc-S strain.

2.6. CFU assays of mycobacterium-infected macrophages and mouse lungs

To evaluate the survival of infected bacteria in BMDMs, Mabc or Mboll-infected cells (MOI 1) were incubated for 2–3 h and washed twice with PBS to eliminate residual bacteria. For the 0-day observation, cells were lysed immediately after washing with PBS. For later time points, cells were incubated in fresh medium containing different concentrations of V46 for specified durations. After PBS or medium had been discarded, cells were lysed by adding 200 μL of sterile distilled water with 0.1 % Tween-80 for 45 min at 37℃ in 5 % CO_2, followed by harvesting of released intracellular bacteria. Cell lysates were serially diluted fivefold in PBST, and 10 μL aliquots were dropped onto Middlebrook 7H10 agar containing 10 % OADC. Colonies were counted to evaluate bacterial survival after incubation for 3 or 5 days at 37℃. To quantify CFUs *in vivo*, lungs were dissected from Mabc-infected mice after 5, 10, or 21 days. Next, lungs were homogenized in 200 μL of PBST, followed by serial dilution. Diluted homogenates were dropped in triplicate 10 μL aliquots onto Middlebrook 7H10 agar with 10 % OADC.

2.7. Reagents

Fluoromount-G Mounting Medium with 4',6-diamidino-2-phenylindole (DAPI) (00–4959–52) was purchased from Invitrogen (Waltham, MA, USA). β-Cyclodextrin (H5784), bafilomycin A1 (Baf-A1; B1793), gentamicin (G1397), 2-mercaptoethanol (M6250), and chloroquine diphosphate salt (CQ; C6628) were purchased from Sigma-Aldrich. For anesthesia, 2,2,2-tribromoethanol, 99 % (AC421430100), was purchased from Acros Organics. For Western blotting, anti-phospho (p)-signal transducer and activator of transcription 3 (STAT3; 9145), anti-STAT3 (9139), anti-p-nuclear factor kappa B (NF-κB; p65) (3033), anti-p65 (8242), anti-p-p38-mitogen activated protein kinase (MAPK) (p-p38; 4511), anti-p38 (8690), anti-p-c-Jun N-terminal kinase (JNK; 4668), anti-JNK (9252), anti-p-extracellular signal regulated kinase (ERK1/2; 9101), anti-ERK1/2 (4695), anti-p-protein kinase B/AKT (4060), anti-AKT (9272), anti-p-adenosine monophosphate (AMP)-activated protein kinase (AMPK; 2535), anti-AMPK (2532), anti-p-mammalian target of rapamycin (mTOR; 5536), anti-MTOR (2983), anti-microtubule-associated protein 1 light chain 3 β (LC3B; L7543), anti-ACTIN (5125), anti-mouse-IgG (7076), and anti-rabbit-IgG (7074) antibodies were purchased from Cell Signaling Technology (Danvers, MA, USA). To measure intracellular Ca^{2+}, Fura-2/AM (F1221) was purchased from Invitrogen. For immunofluorescence, anti-LC3A/B (PM036) was purchased from MBL Co., Ltd. (Tokyo, Japan). Anti-lysosomal-associated membrane protein 1 (LAMP1; sc-19992) was purchased from Santa Cruz Biotechnology (Dallas, TX, USA). Alexa Fluor 488 (anti-rabbit, A110006; anti-rat, A110008) was purchased from Thermo Fisher Scientific (Waltham, MA, USA). Anti-TFEB (A303–673A) was purchased from Bethyl Laboratories, Inc. (Montgomery, TX, USA). CLA, RFB, amikacin (AMK), imipenem (IMP), and cefoxitin (CFX) were purchased from Sigma-Aldrich. Bedaquiline (BDQ) and omadacycline (OMD) were obtained from Adooq Bioscience (Irvine, CA, USA). Resazurin sodium salt (B21187.03) was purchased from Alfa Aesar (Haverhill, MA, USA). Chemicals for the synthesis of RSV derivatives were purchased from Sigma-Aldrich (USA), TCI (Japan), and Duksan Pure Chemistry (South Korea).

2.8. Synthesis of RSV derivatives

During the synthesis of RSV derivatives, we varied the number of substitutions in the RSV core and replaced hydroxy groups with functional groups, resulting in 11 derivatives (Fig. S1). Initially, we synthesized RSV derivatives with a monosubstituent. Compounds **3a-3f** were synthesized through a Heck cross-coupling reaction from aryl bromide and styrene, using a microwave reactor (Supplementary Scheme S1). Next, compound **5**, which exhibits an aldehyde group at

position 2, was prepared by Vilsmeier-Haack reaction of RSV with $POCl_3$ and *N,N*-dimethylformamide (DMF). Subsequently, the methoxylated compound **6** was prepared from compound **5** with K_2CO_3 and methyl iodide, then reacted with $NaBH_4$ to form compound **7**. Compounds **8** (V46) and **9** were synthesized from RSV by methylation with sodium hydride and methyl iodide or acetylation with acetyl chloride and triethylamine, respectively (Supplementary Scheme S2).

2.9. Cell viability assay

Cell viability was measured as previously described [26]. Mabc-infected or -uninfected BMDMs were treated with V46 for 24 or 48 h, followed by the addition of 10 μL Cell Counting Kit-8 (CCK-8) dye for 2 h. Absorbance at 450 nm was measured using a Synergy HT microplate reader (BioTek, Winooski, VT, USA).

2.10. Three-dimensional holographic imaging

BMDMs were seeded in black, six-well, glass-bottom (0.17 ± 0.005 mm) plates (P06–1.5 H-N, Cellvis, Mountain View, CA, USA). Mabc-mWasabi-infected BMDMs (MOI 5) were incubated for 4 h at 37℃. Next, cells were washed twice with PBS, and fresh medium containing either solvent control (SC) or V46 (100 μM) was added. For live-cell imaging, a Tomocube microscope (HT-2 H, Tomocube Inc., Daejeon, South Korea) was used; images were analyzed using TomoStudio software (Tomocube Inc.). Images were automatically acquired 0 or 24 h after treatment with SC or V46 and analyzed using ImageJ software.

2.11. Histology

Lungs were acquired from Mabc-infected WT C57BL/6 or C3HeB/FeJ mice treated with vehicle (n = 3, respectively) or V46 (50 mg/kg, n = 3, respectively) for 21 days, fixed with 10 % formalin, and embedded in paraffin wax. For histopathological analysis, paraffin-embedded lung tissues were sectioned to 4 μm thickness and subjected to hematoxylin-and-eosin (H&E) staining. Images were acquired using the Aprio Digital Pathology Slide Scanner (Leica, Wetzlar, Germany) and the ScanScope CS System (Leica). Whole fields of lung tissue were scanned, and inflamed areas were quantified after determination of the mean fluorescence intensity in the red channel using FIJI software.

2.12. RNA preparation and quantitative real-time polymerase chain reaction (qRT-PCR)

Total RNA was extracted from lung tissue homogenates or BMDMs as previously described [28]. Relative mRNA levels were determined and normalized to *Actb*. Primer sequences are listed in Supplementary Table S1.

2.13. RNA sequencing

Total RNA was extracted from either Mabc-infected murine BMDMs treated with or without V46. Sequencing was conducted using the Illumina NovaSeq 6000 platform (Illumina, Inc., San Diego, CA, USA) with paired-end 100 bp reads. The adaptors and low-quality bases were assessed using FASTQC (version 0.11.7). Trimmed reads were then aligned to the *Mus musculus (mm10)* genome using HISAT (version 2.1.0), based on Bowtie2 implementations. Aligned data (SAM file format) were sorted and indexed using SAMtools (version 1.9). After alignment, the transcripts were assembled and quantified using StringTie (version 2.1.3b). Transcriptomic expression levels were calculated using fragments per kilobase of transcript per million mapped reads and transcripts per million methods. The genes differentially expressed were analyzed by DESeq2 (version 1.38.3) using raw counts as input. Normalized gene read count data were used to generate a heatmap plot with the pheatmap (version 1.0.12). All data analysis and visualization of differentially expressed genes was conducted using R (version 4.2.2). The RNA sequencing data used in this study are available at the Gene Expression Omnibus (accession number: GSE272313).

2.14. Enzyme-linked immunosorbent assay (ELISA)

The levels of the proinflammatory cytokines interleukin (IL)-6 (555240) and IL-1β (BMS6002) were determined in the supernatants of lung lysates or mouse BMDMs using the Mouse BD OptEIA Set ELISA Kit (BD Biosciences) for IL-6 and IL-1β Mouse ELISA Kit (Thermo Fisher Scientific), respectively, in accordance with the manufacturer's instructions.

2.15. Western blotting

Protein samples from BMDM lysates were subjected to 8 % or 12 % sodium dodecyl sulfate–polyacrylamide gel electrophoresis and transferred to nitrocellulose membranes (Pall Corporation, Port Washington, NY, USA, 66485) at 200 mA for 2 h. Membranes were blocked using 1× blocking solution (Biofact, Daejeon, South Korea, op106–500) for 30 min at room temperature (RT) and reacted overnight with an anti-p-STAT3, -STAT3, -p-p65, -p65, -p-p38, -p38, -p-JNK, -JNK, -p-ERK1/2, -ERK1/2, -p-AKT, -AKT, -p-AMPK, -AMPK, -p-MTOR, -MTOR, or -ACTIN primary antibody at 4℃. Next, horseradish peroxidase-conjugated secondary antibodies (7076S [anti-mouse IgG], 7074S [anti-rabbit IgG]; Cell Signaling Technologies) were reacted with the membrane for 1 h at RT. Immunoreactive bands were visualized using the ECL reagent from the Chemiluminescence Assay Kit (Millipore, WBKL S0500) and a UVitec Alliance mini-chemiluminescence device (UVitec, Rugby, UK). Band intensity was analyzed using ImageJ software and normalized to total protein. Raw Western blot images are shown in Figs. S9–S14.

2.16. Measurement of intracellular Ca^{2+} concentration

The intracellular Ca^{2+} concentration was measured as previously described [25].

2.17. Transmission electron microscopy (TEM)

For TEM analysis, Mabc-infected or -uninfected BMDMs were washed with PBS and fixed for 3 h with 0.1 M cacodylate buffer (pH 7.2) containing 2.5 % glutaraldehyde and 0.1 % $CaCl_2$. Post-fixation was conducted with 0.1 M sodium cacodylate buffer containing 1 % OsO_4 and 0.1 % $CaCl_2$. Cells were washed with cold distilled water and slowly dehydrated using an ethanol series and propylene oxide at 4℃. Cells were then embedded in Embed-812 and cured at 60℃ for 30 h. Using a diamond knife and Ultracut UC7 ultramicrotome (Leica), embedded cells were sectioned (70 nm) and mounted on formvar-coated copper grids. Sections were stained with 4 % uranyl acetate for 7 min and lead citrate for 7 min, then scanned using a Bio-High Voltage EM system (JEM-1400 Plus and JEM-1000 BEF; Jeol Ltd., Tokyo, Japan).

2.18. Immunofluorescence analysis

Immunofluorescence analysis was conducted as described elsewhere [14]. Primary antibodies (anti-LC3, 1:400 diluted; anti-TFEB, 1:400 diluted; anti-LAMP1, 1:400 diluted) and secondary antibodies (anti--rabbit or anti-rat IgG-Alexa Fluor 488 Ab, 1:400 diluted) were used after appropriate dilution. Cells were mounted using Fluoromount-G Mounting Medium with DAPI. Fluorescence images were collected with a confocal laser-scanning microscope (for LC3 and TFEB, Zeiss, LSM-900; for LAMP1, Stella 5, Leica) and analyzed using ImageJ software. To investigate autophagic flux in BMDMs, cells were transduced with retroviruses expressing tandem-tagged mCherry-enhanced green fluorescent protein (EGFP)-LC3B for 24 h, treated with V46 in the presence or absence of Baf-A1 for 24 h, and visualized by confocal microscopy.

2.19. Production of tandem LC3B retroviral plasmids

To evaluate autophagic flux, a tandem LC3B retroviral plasmid (mCherry-EGFP-LC3B) was generated [29]. Phoenix amphotropic cells were co-transfected with 0.75 μg of the packaging plasmid pCL-Eco (Addgene, Watertown, MA, USA; 12371), 0.25 μg of the envelope plasmid pMDG (Addgene, 187440), and 1 μg of pBABE-puro mCherry-EGFP-LC3B plasmid (Addgene, 22418) using Lipofectamine 2000 Transfection Reagent (Invitrogen, 11668019), in accordance with the manufacturer's instructions. After 6 h, the medium was replaced with fresh medium. Retrovirus-containing supernatant was collected at 24 and 48 h post-transfection and passed through a 0.45-μm sterile syringe filter (Millipore, Billerica, MA, USA; SLHV004SL).

2.20. Transduction of lentiviral shRNA

To silence *Tfeb* in BMDMs, we obtained three packaging plasmids (containing pMDLg/pRRE [12251], pRSV-Rev [12253], pMD2, VSV-G [12259], and *Tfeb* [sc-38510-SH] shRNA; Addgene and Santa Cruz Biotechnology, respectively). Plasmids were simultaneously transfected into HEK293T cells using Lipofectamine 2000 Transfection Reagent (Invitrogen). After 72 h, culture supernatant was collected, centrifuged at 626 × g for 5 min to remove cells, and passed through a 0.45-μm filter (Millipore, SLHV004SL). Lentivirus was collected by ultracentrifugation at 107,000 × g for 2 h at 4℃. Viral pellets were gently resuspended in chilled PBS, aliquoted, and stored at −80℃. BMDMs were seeded in 48-well plates, transduced with lentiviral plasmids for 1 day, then incubated in fresh medium for 3 days. Transduction efficiency was evaluated by qRT-PCR using primers targeting *Tfeb*.

2.21. Microinjection of Mabc into embryos and analysis of drug effectiveness

ZF eggs were dechorionated, and ZF larvae were anesthetized with tricaine (270 mg/L). Mabc inoculum (with PBST and phenol red) was injected into the caudal vein using a Tritech Research Digital micro-INJECTOR (MINJ-D; Tritech Research, Los Angeles, CA, USA). Next, 20 infected ZF were cultured in blue fish water with methylene blue (1 g/L) at 28.5°C in 96-well plates (two embryos per well) to track infection kinetics and larval survival. For *in vivo* efficacy assessment, the maximum tolerated dose was determined. Infected larvae were treated with V46 (0.2, 0.4, 0.75, 1.5, and 3.0 μM). For the combination study, GFP-Mabc infected ZF were treated with vehicle, CLA (50 μM), or V46 (0.75, 1.5, and 3 μM) in the presence or absence of CQ (1 μM). Uninfected and infected but untreated ZF served as controls. Fresh fish water and compounds were replaced daily. To evaluate survival, dead embryos (i.e., those without a heartbeat) were monitored daily for 13 days.

To analyze bacterial burden, ZF (5 days post-infection [dpi]) were individually homogenized in 2 % Triton X-100–PBST using a 26-gauge needle. Several 10-fold dilutions of suspension in PBST were dropped on 7H10 agar containing 50 μg/mL kanamycin and BBL MGIT PANTA (polymyxin B, amphotericin B, nalidixic acid, trimethoprim, and azlocillin; Becton Dickinson, Franklin Lakes, NJ, USA) to prevent fungal growth. Plates were incubated for 5 days, and CFUs were enumerated [30]. GFP-Mabc evolution was assessed by visualizing GFP expression in larvae using the ImageXpress Pico Automated Cell Imaging System (Molecular Devices, Sunnyvale, CA, USA) to capture images via fluorescence microscopy. Survival curves were created using Prism 8.0 software and subjected to Kaplan–Meier analysis and the log-rank (Mantel–Cox) test.

2.22. Determination of minimal inhibitory concentration (MIC) by REMA and REMA checkerboard assay

MIC values were determined by REMA as previously described [31]. To identify synergistic, antagonistic, and additive effects of V46 combinations against Mabc, a checkerboard assay was performed using REMA as previously described [32,33]. Briefly, 1 μL of twofold serial dilutions of V46 (the lowest was eightfold greater than the MIC_{50}) was prepared in a 96-well microplate (98 μL per well) (Corning, Baltimore, MD, USA) and interacted with seven anti-Mabc drugs (CLA, RFB, AMK, CFX, OMD, BDQ, and IMP) at the indicated concentrations. The exponential-phase Mabc inoculum was adjusted to an OD600 of 0.0025 and added to the plates to achieve a total volume of 100 μL. Plates were incubated for 3 days at 37°C, followed by the addition of resazurin (0.025 % [w/v] to 10 % of the well volume). After overnight incubation, fluorescence intensity was measured using a SpectraMax M3 multimode microplate reader (Molecular Devices) with excitation at 560 nm and emission at 590 nm. Experiments were performed in triplicate. To evaluate interactions among the compounds, the following formula was used to calculate fractional inhibitory concentrations (FICs): FIC (X + Y) = [MIC of compound X in combination with Y] ÷ [MIC of X alone]. The fractional inhibitory index (∑FIC) was regarded as the cumulative FICs of compounds X and Y: ∑FIC < 0.5, synergistic; 0.5 < ∑FIC < 1, additive; 1 < ∑FIC < 2, indifference; and ∑FIC ≥ 2, antagonistic [34]. Bacteria incubated with the drug combinations were spotted on 7H10 agar, incubated for 5 days, and subjected to CFU enumeration.

2.23. Statistical analysis

Statistical analysis was performed using Prism 8.0 software for Windows (GraphPad Software Inc., San Diego, CA, USA). The two-tailed Student's *t*-test or Mann-Whitney U test was used to compare two groups, and one-way analysis of variance (ANOVA) was applied to compare three or more groups. Data are presented as means ± standard deviations (SDs) or standard errors of the mean (SEMs). Values of $p < 0.05$ were considered statistically significant.

3. Results

3.1. V46 exerted an antimicrobial effect in macrophages infected with Mabc

We designed and synthesized 11 RSV derivatives (Figs. S1 and 1A) and evaluated their inhibitory activities on intracellular bacterial survival in Mabc-infected BMDMs (Fig. 1B). Two RSV derivatives, *trans*-3,5,4′-trimethoxystilbene (compound 8; **V46**) and (*E*)-5-(4-acetoxystyryl)-1,3-phenylene diacetate (compound 9), reduced intracellular bacterial viability in BMDMs (Fig. 1B). V46 significantly inhibited the intracellular growth of Mabc (Fig. 1B). Based on these results, we conducted structure activity relationship study. The presence of functional groups at positions 3, 4′, and 5 in RSV significantly influenced its activity. Substitution of the hydroxy group with a methoxy group markedly enhanced activity. These findings provide crucial insights for structural modifications aimed at improving activity for subsequent development. Next, we assessed the cytotoxicity of V46 against BMDMs by CCK-8 assay (Fig. S2). At 200 μM, V46 showed minimal cytotoxicity against Mabc-infected BMDMs, indicating a favorable safety profile.

We compared the antimicrobial activities of original RSV and V46 by evaluating bacterial survival in Mabc-infected BMDMs treated with each compound (Fig. 1C). V46 exhibited significantly enhanced antimicrobial activity in a dose-dependent manner against intracellular Mabc in BMDMs (Fig. 1C). Importantly, V46 exerted a stronger anti-Mabc effect in BMDMs compared to RSV (Fig. 1C) and effectively inhibited intracellular bacterial replication after 18 h (Fig. 1D). Additionally, V46 showed a similar dose-dependent antimicrobial effect in Mabc-infected hMDMs (Fig. 1E). V46 also exerted a significantly greater (compared with RSV) antimicrobial effect against Mabc-S in BMDMs (Fig. 1F) and reduced intracellular survival of Mboll in BMDMs in a dose-dependent manner (Fig. 1G). We next determined the antimicrobial activity of V46 against intracellular Mabc at the individual-cell level using three-dimensional holographic imaging (Fig. 1H). Initial bacterial numbers were similar (Fig. S3A and B), and V46 treatment for 24 h significantly

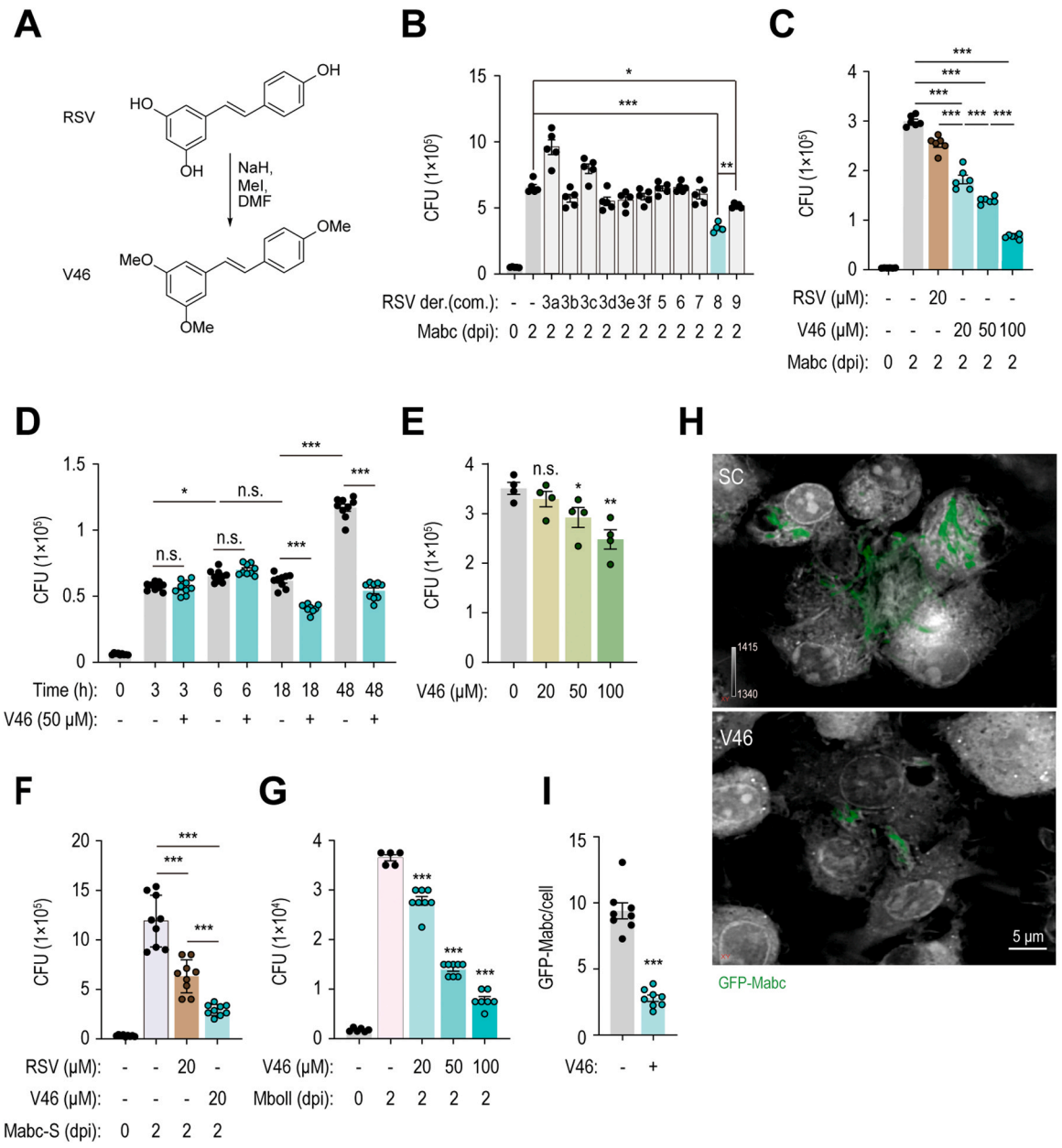

Fig. 1. V46 exerts an antimicrobial effect during Mabc or MboII infection *in vitro*. **(A)** Structure and synthesis schematic diagram of V46 from RSV. **(B)** Intracellular survival assay. Mabc-infected (MOI 1) BMDMs treated with 11 RSV derivative compounds (20 μM) for 2 days (3a: tri-stilbene, 3b: 2-hydroxystilbene, 3c: 3-hydroxystilbene, 3d: 4-hydroxystilbene, 3e: 3-acetylstilbene, 3 f: 4-acetylstilbene, 5: (*E*)-2,4-dihydroxy-6-(4-hydroxystyryl)benzaldehyde, 6: (*E*)-2,4-dimethoxy-6-(4-methoxystyryl)benzaldehyde, 7: (*E*)-(2,4-dimethoxy-6-(4-methoxystyryl)phenyl)methanol, 8: *trans*-3,5,4′-trimethoxystilbene (V46), 9: (*E*)-5-(4-acetoxystyryl)-1,3-phenylene diacetate). Mabc-infected BMDMs were lysed after treatment with RSV derivatives (2 dpi) or only Mabc infection (0 or 2 dpi). **(C)** Intracellular survival in Mabc-infected (MOI 1) BMDMs treated with RSV (20 μM) or V46 (20, 50, and 100 μM) for 2 days. **(D)** Intracellular survival in Mabc-infected (MOI 1) BMDMs treated with or without V46 (50 μM) for the indicated times. **(E)** Mabc-infected (MOI 1) hMDMs were treated or not with V46 (20, 50, and 100 μM) for 2 days post-infection. **(F)** Mabc-S-infected (MOI 1) BMDMs were treated or not with RSV or V46 (20 μM) for 2 days post-infection. **(G)** MboII-infected (MOI 1) BMDMs were treated or not with V46 (20, 50, and 100 μM) for 2 days post-infection. **(H and I)** *In vitro* antimicrobial activity of V46 using GFP-Mabc. BMDMs infected with GFP-Mabc (MOI 5) were washed with PBS twice after 4 h, and medium was replaced with fresh medium containing SC or V46 (100 μM) for 24 h. Intracellular GFP-Mabc visualized using a holotomographic microscope. Representative images from three independent experiments are shown. Quantitative analysis of GFP-Mabc per cell using six independent images per group. Experiments involved three biological replicates. Statistical analysis conducted by one-way ANOVA with Tukey's multiple comparison test (B-D, F, and G) or two-tailed Student's *t*-test (E and I). Information on RSV compounds (3a to 9) is provided in the Supplementary Materials. Data from at least three independent experiments are shown with error bars (means ± SDs or SEMs). CFU, colony-forming unit; RSV, resveratrol; der., derivatives; com., compound; Mabc, *Mycobacteroides abscessus*; dpi, days post-infection; SC, solvent control; Mabc-S, *Mycobacteroides abscessus* smooth-type variants; GFP, green fluorescent protein; n.s., not significant. $^{*}p < 0.05$, $^{**}p < 0.01$, and $^{***}p < 0.001$.

reduced the increase in GFP-Mabc numbers in BMDMs compared with the SC (Fig. 1H and I). V46 also led to the appearance of bacterial fragments in GFP-Mabc-infected cells (Fig. 1H). Therefore, these data strongly suggest that, among RSV derivatives, V46 is notably effective in exerting intracellular antimicrobial activity against Mabc growth.

3.2. V46 is effective in exerting antimicrobial activity against Mabc infection in vivo

To evaluate the *in vivo* effect of V46, C57BL/6 mice were intranasally infected with Mabc (1×10^6 CFUs per mouse) and treated with either

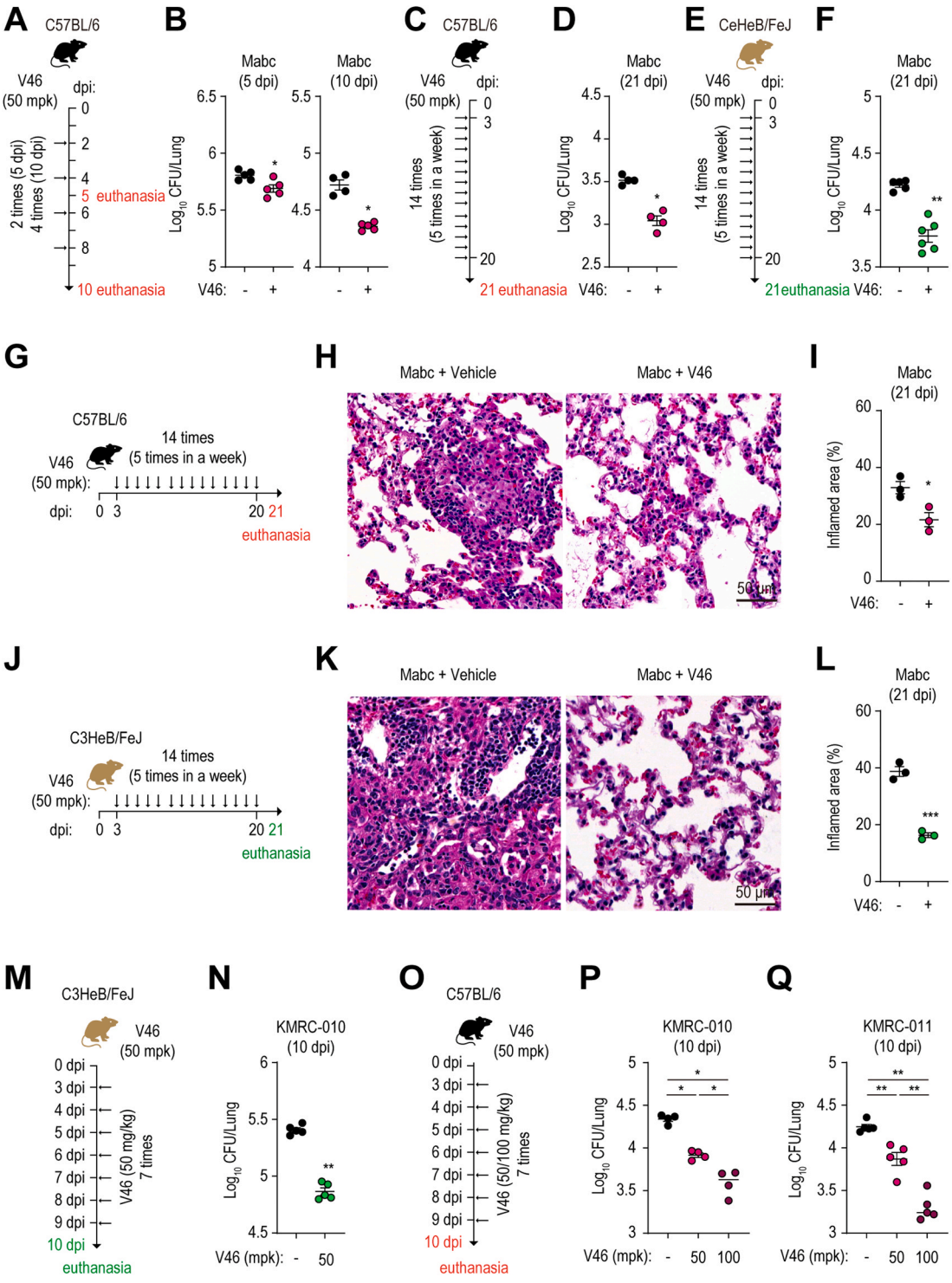

Fig. 2. V46 exerts an antimicrobial effect against Mabc infection *in vivo*. **(A-F)** Mice (C57BL/6 **[A-D]**; C3HeB/FeJ **[E-F]**) were intranasally infected with Mabc (1×10^6 CFUs for C57BL/6 or 1×10^3 CFUs for C3HeB/FeJ); n = 4–6 per group), intraperitoneally treated with vehicle or V46 (50 mg/kg), and euthanized. At 5, 10 **(A and B)**, or 21 **(C-F)** dpi, lungs were homogenized and subjected to CFU counting. **(G-L)** Mice (C57BL/6 **[G-I]**; C3HeB/FeJ **[J-L]**; n = 3 per group) were intranasally infected with Mabc (1×10^6 CFUs for C57BL/6 or 1×10^3 CFUs for C3HeB/FeJ) and intraperitoneally treated with vehicle or V46 (50 mg/kg). At 21 dpi, lungs were collected to assess the inflamed region. Representative H&E-stained histopathological images and quantitative analysis of the inflamed area of lung tissues from mice are shown. **(M-Q)** C3HeB/FeJ **(M and N)** or C57BL/6 **(O-Q)** mice (n = 5 per group) were intranasally infected with KMRC-010 **(N and P)** or KMRC-011 **(Q)** (1×10^5 CFUs/mouse), respectively, and intraperitoneally treated with vehicle or V46 (50 or 100 mg/kg) at 3–9 dpi, and euthanized. At 10 dpi, lungs were homogenized and subjected to CFU counting. Statistical analysis was conducted by the Mann-Whitney U test (B, D, F, N, P, and Q) or two-tailed Student's *t*-test (I and L). All experimental schedule is pictured as schematic diagrams in A, C, E, G, J, M, and O. Data from at least three independent experiments are shown with error bars (means ± SEMs). CFU, colony-forming unit; Mabc, *Mycobacteroides abscessus*; dpi, days post-infection; mpk, milligram per kilogram. $*p < 0.05$, $**p < 0.01$, and $***p < 0.001$.

vehicle or V46 (50 mg/kg). V46 exhibited potent antimicrobial activity against Mabc during both early (5 and 10 days; Fig. 2A and B) and late (21 days; Fig. 2C and D) stages of infection. The lung Mabc CFU count in the V46-treated group (50 mg/kg) was significantly lower than that in the vehicle-treated control group (Fig. 2B and D). CFU counts in the lungs of Mabc (1×10^3 CFUs per mouse)-infected C3HeB/FeJ mice, which are more susceptible to mycobacterial infection [35], were lower in the V46-treated group than in the vehicle-treated control group (Fig. 2E and F). Furthermore, V46 significantly reduced the number of pathological granulomatous lesions in the lungs of Mabc-infected C57BL/6 (Fig. 2G-I) and C3HeB/FeJ mice (Fig. 2J-L) compared with vehicle-treated controls.

To investigate the protective effect of V46 against infection with clinical strains of Mabc resistant to multiple drugs (including rifampicin, ethambutol, and CLA), we evaluated *in vivo* CFU counts of MDR-Mabc strains, KMRC-010 and KMRC-011, in the lungs of vehicle- and V46-treated C3HeB/FeJ or C57BL/6 mice (Fig. 2M-Q). V46 treatment significantly reduced CFU counts in the lungs of KMRC-010-infected C3HeB/FeJ (Fig. 2M and N; 1×10^5 CFUs/mouse) and C57BL/6 mice (Fig. 2O and P; 1×10^5 CFUs/mouse) compared to vehicle-treated controls. This *in vivo* CFU reduction effect of V46 was also observed in KMRC-011-infected C57BL/6 mice (Fig. 2O and Q; 1×10^5 CFUs/mouse). Thus, V46 effectively reduced Mabc load and mitigated pathological pulmonary responses in infected mice.

3.3. V46 alleviates Mabc-induced inflammatory responses both in macrophages and in vivo

We investigated the effect of V46 on inflammatory responses by analyzing cytokine and chemokine expression levels in Mabc-infected BMDMs. Differentially expressed genes in Mabc-infected BMDMs with SC or V46 treatment (Fig. 3A) included several chemokine genes (such as *Cxcl2* and *Ccl3*) and cytokine genes (such as *Il6* and *Il1b*). Mabc infection significantly increased gene expression of *Cxcl2*, *Ccl3*, *Cxcl1*, *Ccl4*, *Il6*, and *Il1b*. However, V46 treatment of Mabc-infected BMDMs resulted in a dose-dependent decrease in mRNA levels of these chemokines and cytokines after 6 h (Fig. 3B). TNF-α is important in neutrophil trafficking and granuloma formation, but its role in reducing lung bacterial load is unclear [36]. Intriguingly, V46 did not modulate TNF-α signaling during Mabc infection (Fig. S4).

Consistent with the gene expression results, V46 reduced the production of IL-6 and IL-1β in Mabc-infected BMDMs compared with the SC group, starting at 6 h of treatment (Fig. 3C and S5). To evaluate the impact of V46 on lung inflammatory responses to Mabc infection, mice were infected with Mabc (1×10^6 CFUs/mouse) and treated with either vehicle or V46 (50 mg/kg). V46 significantly reduced the mRNA levels of chemokines (*Cxcl2*, *Ccl3*, *Cxcl1*, and *Ccl4*) and cytokines (*Il1b* and *Il6*) in the lungs of Mabc-infected mice at 5 and 10 dpi (Fig. 3D). Moreover, V46 treatment of Mabc-infected mice significantly decreased IL-6 and IL-1β protein levels in lung lysate supernatants compared with vehicle controls (Fig. 3E). Due to the involvement of mycobacterium-induced IL-6 production and the JAK-STAT3 signaling pathway in host responses to bacterial infection [37,38], we investigated whether V46 modulated STAT3 activation in Mabc-infected BMDMs (Fig. 3F). Immunoblotting showed that the strong activation of STAT3 in BMDMs at 18 h after infection with Mabc was significantly reduced by V46. Additionally, V46 decreased STAT3 phosphorylation in the lungs of MDR-Mabc (KMRC-010)-infected mice (Fig. 3G). Taken together, these findings suggest that V46 modulates the host inflammatory response to Mabc infection.

3.4. V46 inhibits the AKT-mTOR pathway, while enhances AMPK signaling during Mabc infection

To investigate the molecular mechanisms underlying the effect of V46 on inflammatory signaling, we examined the activation of key signaling pathways involved in innate immunity and mycobacterial infection [12,39].

V46 significantly suppressed AKT activation during Mabc infection (Fig. 4A and B). However, V46 had no or only mild effect on other signaling factors, including p-p65, p-p38, p-JNK, and p-ERK1/2 levels (Fig. 4A and S6). Notably, AKT inhibits AMPK activation, a metabolic kinase that senses the AMP:ATP ratio [40]. Accordingly, we evaluated the activation of AMPK and its downstream target, mTOR. V46 significantly increased AMPK activity from early time points and decreased mTOR activity at 0.5 and 1 h (Fig. 4C–F). AMPK activation is influenced by intracellular Ca^{2+} levels during mycobacterial infection [41,42]. Therefore, we investigated the effect of V46 on intracellular Ca^{2+} levels in Mabc-infected BMDMs (Fig. 4G and H). V46 increased intracellular Ca^{2+} levels in Mabc-infected BMDMs by approximately 1.5-fold compared with those in the SC (Fig. 4H). Collectively, these results indicate that V46 suppresses AKT-mTOR signaling and enhances Ca^{2+}-AMPK signaling during Mabc infection.

3.5. V46 activates autophagic flux in macrophages

Considering that AMPK activation promotes autophagy by inhibiting mTOR and AKT [43,44], we investigated whether the antimicrobial effect of V46 is mediated by autophagy induction. V46 treatment significantly increased LC3 puncta numbers in BMDMs (Fig. 5A and B) and hMDMs (Fig. 5C and D) after 6 h. TEM analysis confirmed autophagy induction by treating V46, evidenced by increased autophagosomal structures in V46-treated BMDMs (Fig. 5E and F). Additionally, V46 with Baf-A1, a lysosomal vacuolar H+-ATPase inhibitor [45,46], resulted in LC3B-II accumulation, indicating enhanced autophagic flux (Fig. 5G and H).

To confirm that V46 induces autophagic flux, we transduced BMDMs with a retroviral vector containing mCherry-EGFP-LC3B [38] and treated them with V46. The number of red punctate structures (mCherry; resistant to acidic conditions), indicative of autolysosomes (where acidic pH suppresses GFP fluorescence), increased with V46 treatment. However, pre-treatment with Baf-A1 inhibited this effect in V46-treated BMDMs (Fig. 5I and J). Thus, V46 effectively activates autophagic flux in BMDMs.

3.6. V46 activates autophagy to promote antimicrobial host defenses against Mabc

We then investigated whether V46-induced autophagy promotes Mabc-containing autophagosome formation and antimicrobial activity. BMDMs were infected with GFP-Mabc, treated with either SC or V46, and evaluated for LC3-positive autophagosome colocalization with GFP-Mabc. Colocalization of LC3 and GFP-Mabc significantly increased in V46-treated compared with those in SC-treated BMDMs (Fig. 6A and B). We evaluated Mabc subcellular localization by TEM as described elsewhere [47–50]. *Cytosolic mycobacteria* are bacilli not surrounded by a phospholipid bilayer; *phagosomal mycobacteria* are bacilli enclosed within a single host phagosomal membrane; and *autophagosomal mycobacteria* are bacilli contained within double or multiple, onion-like vacuolar structures (Fig. 6C-E). V46-treated BMDMs showed a significant increase in Mabc-containing autophagosomal structures compared with those from SC-treated cells (Fig. 6C-E). Additionally, V46 significantly enhanced Mabc-containing phagosome association with LAMP1, a late endosomal marker, indicating improved phagosomal maturation (Fig. 6F and G).

To determine whether V46-induced autophagy contributes to antimicrobial responses to Mabc infection, we infected BMDMs from *Atg7* WT and cKO mice with Mabc in the presence or absence of V46 and assessed intracellular bacterial survival. Intriguingly, V46 treatment failed to suppress intracellular Mabc growth in *Atg7* cKO BMDMs (Fig. 6H), highlighting the importance of autophagy in V46-mediated antimicrobial activity. Collectively, these data show that V46-

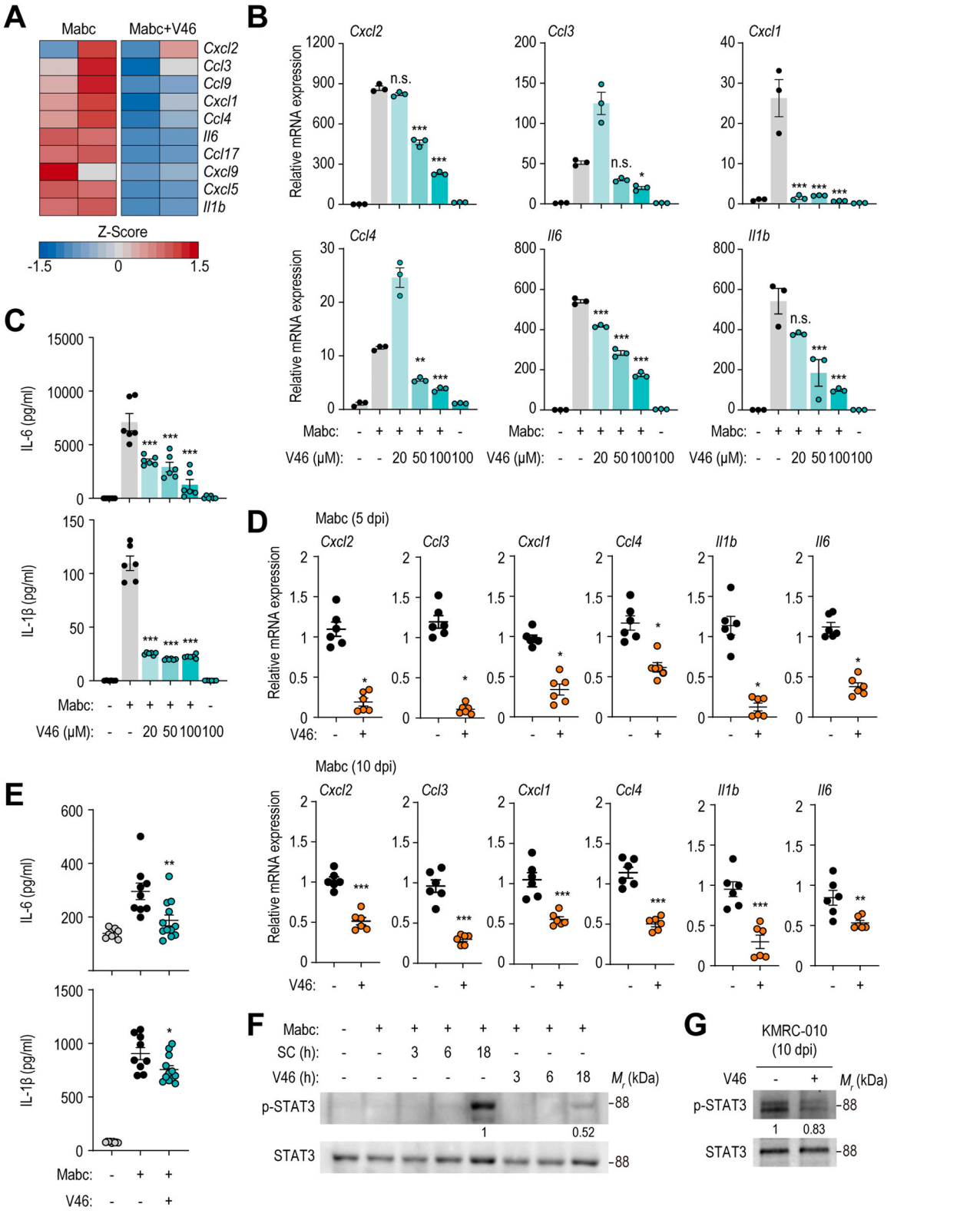

(caption on next page)

Fig. 3. V46 suppresses proinflammatory cytokine and chemokine expression in Mabc-infected murine macrophages and lungs. **(A)** Heatmap of differentially expressed genes in Mabc-infected (MOI 3) BMDMs treated with SC or V46 (100 μM). **(B)** BMDMs were infected with Mabc (MOI 3) or left uninfected for 2 h. SC or increasing concentrations of V46 were then added via medium exchange. Cells were then collected at 6 h post infection, and subjected to qRT-PCR analysis of *Cxcl2*, *Cxcl3*, *Cxcl1*, *Ccl4*, *Il6*, and *Il1b*. Representative data from repeated experiments are shown. **(C)** Supernatants from **(B)**, collected at 18 h post-infection, were subjected to ELISA to measure IL-6 and IL-1β protein levels. **(D)** WT C57BL/6 mice were intranasally infected with Mabc (1×10^6 CFUs/mouse, n = 5 per group) and intraperitoneally treated with vehicle or V46 (50 mg/kg). Mice were euthanized at 5 and 10 dpi. Lung lysates were used to estimate relative expression levels of chemokines (*Cxcl2*, *Ccl3*, *Cxcl1*, and *Ccl4*) and cytokines (*Il1b* and *Il6*) by qRT-PCR. **(E)** Supernatants of lung lysates from **(D)** were used to measure IL-6 and IL-1β levels by ELISA (n = 3 mice/group). **(F)** After 2 h of Mabc infection (MOI 1), BMDMs were washed with PBS, incubated in fresh medium, and treated with SC or V46 (100 μM) for the indicated times. **(G)** C57BL/6 mice (n = 3 per group) were intranasally infected with KMRC-010 (1×10^5 CFU per mouse). Mice were intraperitoneally treated with vehicle or V46 (50 mg/kg) at 3–9 dpi and euthanized. Cell lysates **(F)** or homogenized lung lysates from mice **(G)** were subjected to Western blotting using antibodies against p-STAT3 and STAT3. p-STAT3 levels were measured by densitometry and are shown below the image. Statistical analysis was conducted by one-way ANOVA with Tukey's multiple comparison test (B, C, and E) or two-tailed Student's *t*-test (D). Data are from at least three independent experiments. Graphs and Western blot images represent three independent experiments. Error bars indicate ± SD or SEM. Mabc, *Mycobacteroides abscessus*; dpi, days post-infection; SC, solvent control; n.s., not significant. $*p < 0.05$, $**p < 0.01$, and $***p < 0.001$.

mediated activation of autophagy enhances the clearance rate of Mabc infected within macrophages via the phagosomal maturation.

3.7. V46 induces nuclear translocation of TFEB and expression of autophagy genes during Mabc infection

V46 significantly inhibited the phosphorylation of mTOR and AKT in Mabc-infected BMDMs (Fig. 4A and E). These kinases are key regulators of the transcriptional activation and nuclear translocation of TFEB, a master regulator of autophagy and lysosomal biogenesis [51,52]. Consequently, we investigated whether *Tfeb* expression was affected in Mabc-infected BMDMs. Mabc infection downregulated *Tfeb* expression, while V46 significantly upregulated it in these cells (Fig. 7A). Immunostaining showed that Mabc infection significantly inhibited TFEB nuclear translocation in both BMDMs (Fig. 7B and C) and hMDMs (Fig. S7A and B). In contrast, V46 markedly promoted TFEB nuclear translocation at both 0.5 (Fig. 7C and Fig. S7A and B) and 2 h post-treatment (Fig. 7C). Furthermore, V46 dose-dependently upregulated transcript levels of TFEB target genes involved in autophagy and lysosomal biogenesis (Fig. 7D), including *Rab7*, *Lamp1*, *Uvrag*, and *Map1lc3b* [53,54] in Mabc-infected BMDMs.

Moreover, the V46-induced suppression of intracellular Mabc growth was reversed by *Tfeb*-targeting shRNA (sh*Tfeb*) with a transduction rate of approximately 70 % (Fig. 7E and F). This reversal, unlike the effect of nonspecific shRNA (sh*NS*), was attributed to the knockdown of *Tfeb* (Fig. 7E and F). These findings suggest that V46 enhances TFEB nuclear translocation and activates the transcriptional activation of autophagy-related genes, potentially enhancing autophagy and lysosomal function in response to Mabc infection in macrophages.

3.8. V46 activity is independent of SIRT1 and SIRT3 during Mabc infection

RSV acts as an agonist of SIRT1 or SIRT3, which regulate numerous biological functions [55,56]. We therefore investigated whether the effects of V46 are dependent on SIRT1 or SIRT3. To investigate this, we assessed *Sirt1* and *Sirt3* expression levels in both Mabc-infected and uninfected BMDMs treated with SC or V46. Mabc infection did not affect *Sirt1* and *Sirt3* expression at 6 and 18 h (Fig. 8A and B). However, V46 upregulated *Sirt1* and *Sirt3* mRNA levels in a dose-dependent manner in Mabc-infected BMDMs at 18 h compared to SC-treated controls (Fig. 8A and B).

We also evaluated the impact of V46 on intracellular Mabc growth in *Sirt1* WT and KO BMDMs, as well as in *Sirt3* WT and KO BMDMs. Notably, the suppression of intracellular Mabc growth by V46 was similar in both *Sirt1* WT and KO BMDMs (Fig. 8C) and in *Sirt3* WT and KO BMDMs (Fig. 8D). These findings strongly suggest that the antimicrobial effect of V46 is independent of SIRT1 and SIRT3 activity.

3.9. The antimicrobial activity of V46 depends on autophagy in a ZF model

We investigated whether V46 protects against Mabc infection using a ZF model [19]. The *in vivo* efficacy of V46 was evaluated in three ways. First, GFP-Mabc dispersal in ZF at 5 dpi was examined by fluorescence microscopy. GFP-Mabc-infected ZF were treated with vehicle, CLA, or V46 (0.2, 0.4, 0.75, 1.5, and 3 μM) for up to 5 dpi. GFP-Mabc numbers significantly increased, primarily within brain areas, in vehicle-control ZF (Fig. 9A). V46 significantly reduced GFP fluorescence intensity. ZF treated with 3 μM V46 exhibited a weak GFP signal, indicating bacterial growth suppression (Fig. 9A).

Second, we quantified bacterial burden in V46-treated ZF embryos. V46 led to a dose-dependent reduction in the number of CFUs per embryo, and 3 μM V46 had an effect comparable to that of 50 μM CLA (Fig. 9B). Therefore, V46 inhibited Mabc proliferation in ZF. Finally, we assessed the effect of V46 treatment for 14 days on Mabc-infected ZF lifespan. ZF in the vehicle-treated group died at 11 dpi (Fig. 9C). However, V46 significantly prolonged ZF lifespan in a dose-dependent manner. The survival rate increased from 30 % at 1.5 μM V46 to 65 % at 3 μM V46, comparable to the 50 μM CLA-treated group.

To investigate the role of autophagy in the anti-Mabc activity of V46, we treated Mabc-infected ZF with CQ, an autophagy pathway inhibitor. ZF were injected with GFP-Mabc and treated with vehicle, CLA, or V46 (0.75, 1.5, and 3 μM) in the presence or absence of CQ (1 μM). Notably, ZF groups treated with V46 plus CQ exhibited significantly greater GFP signal intensities and viable bacterial loads compared with the control groups (Fig. 9D and E). Consistent with the CFU findings (Fig. 9E), CQ-treated ZF showed significantly decreased survival rates in response to all V46 concentrations during Mabc infection compared with control groups (Fig. 9F). Therefore, the antimicrobial activity of V46 against Mabc infection in the ZF model is autophagy-dependent.

We next explored the effects of drug combinations against Mabc infection *in vitro*. We first determined the MIC_{50} values of various compounds by REMA assay (Table 1). Checkerboard assays showed that the combination of 10.1 M V46 (one-half the MIC_{50}) and RFB (one-half the MIC_{50}) suppressed Mabc growth (Fig. 9G). Similarly, one-quarter the MIC_{50} of V46 and RFB inhibited Mabc growth. To assess the effects of V46-RFB combination ratios on Mabc, we calculated the FIC index (Table 1). The V46-RFB combination exerted the greatest synergistic effect against Mabc, with an FIC index of 0.46 (Table 1).

Colony counting validated the synergistic effect of V46 and RFB shown by checkerboard assays (Fig. 9H). The V46-RFB combination caused a reduction of 5.2 $\log_{10}$ CFUs/mL compared with the SC on day 5. Compared with the SC, V46 alone, or RFB alone, the V46-RFB combination caused a reduction of approximately 3 $\log_{10}$ CFUs/mL. Bactericidal activity was defined as a reduction of ≥ 3 $\log_{10}$ in total CFUs/mL [57]. Therefore, the V46-RFB combination had a synergistic bactericidal effect on Mabc. In contrast, V46 combined with other drugs showed additive inhibitory effects on Mabc growth (Fig. S8A-F).

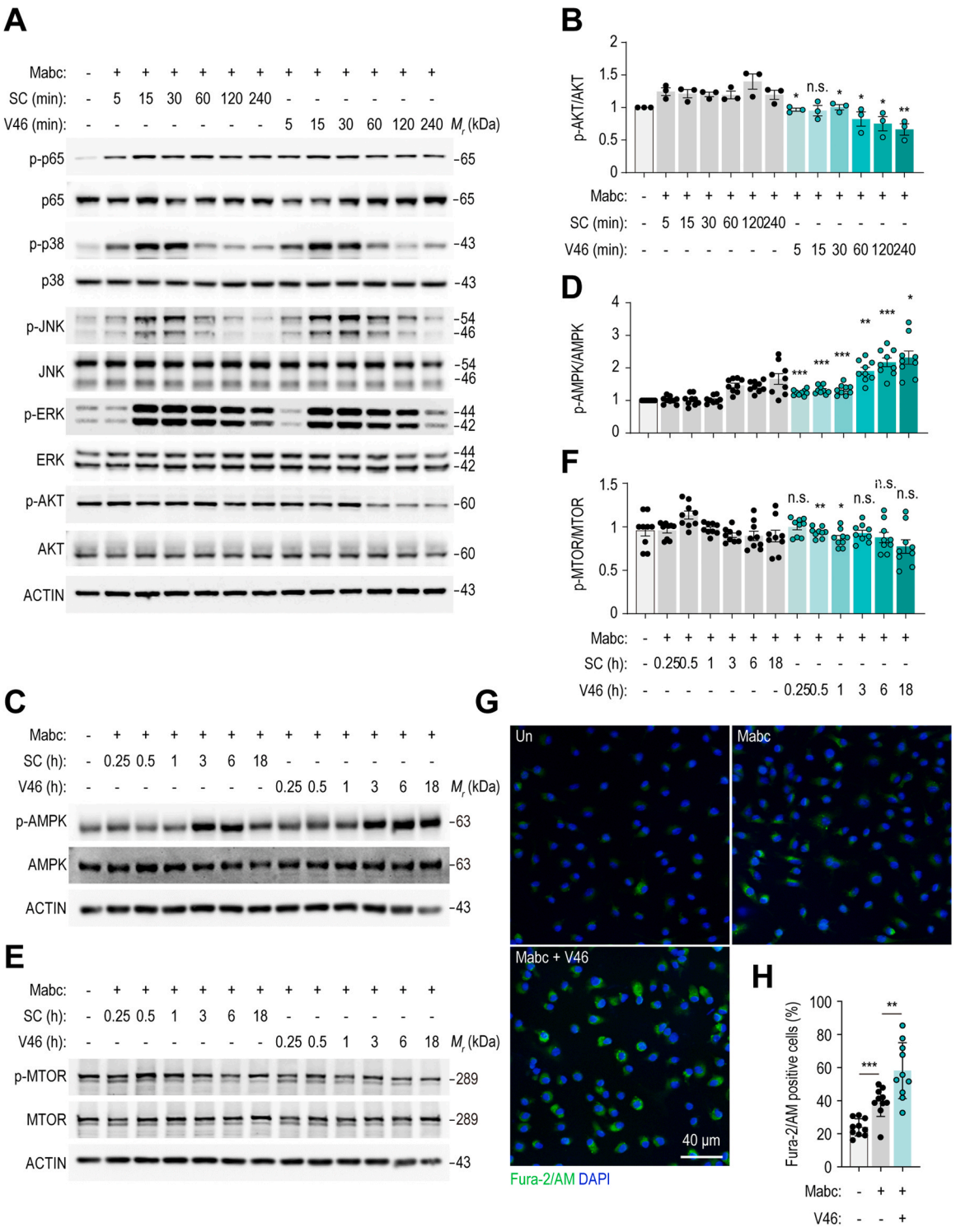

Fig. 4. V46 inhibits activation of the AKT-mTOR signaling pathway and activates AMPK in Mabc-infected murine macrophages in a Ca^{2+}-dependent manner. **(A and B)** BMDMs were pre-treated with SC or V46 (100 μM) for 1 h and infected with Mabc (MOI 1) or left uninfected for the indicated times. **(C-F)** Uninfected or Mabc-infected BMDMs (MOI 1) were incubated for 2 h, washed with PBS, and transferred to fresh medium containing SC or V46 (100 μM) for the indicated times. **(A-F)** Cell lysates were subjected to Western blotting. Densitometry of p-AKT **(B)**, p-AMPK **(D)**, and p-MTOR **(F)** was conducted and normalized to respective total protein bands. **(G and H)** BMDMs were pre-treated with Fura-2/AM (2 μM) for 20 min, infected with Mabc (MOI 1) for 2 h, and treated with SC or V46 (100 μM) for 1 h; fluorescence intensity was measured as indicated in the figure. Fifty cells in each of 10 fields from three experiments were enumerated. Statistical analysis was performed by two-tailed Student's *t*-test (B, D, and F) or one-way ANOVA with Tukey's multiple comparison test (H). Images represent three independent experiments. Error bars denote means ± SEMs or SDs. Mabc, *Mycobacteroides abscessus*; SC, solvent control; n.s., not significant; Un, untreated and uninfected. $*p < 0.05$, $**p < 0.01$, and $***p < 0.001$.

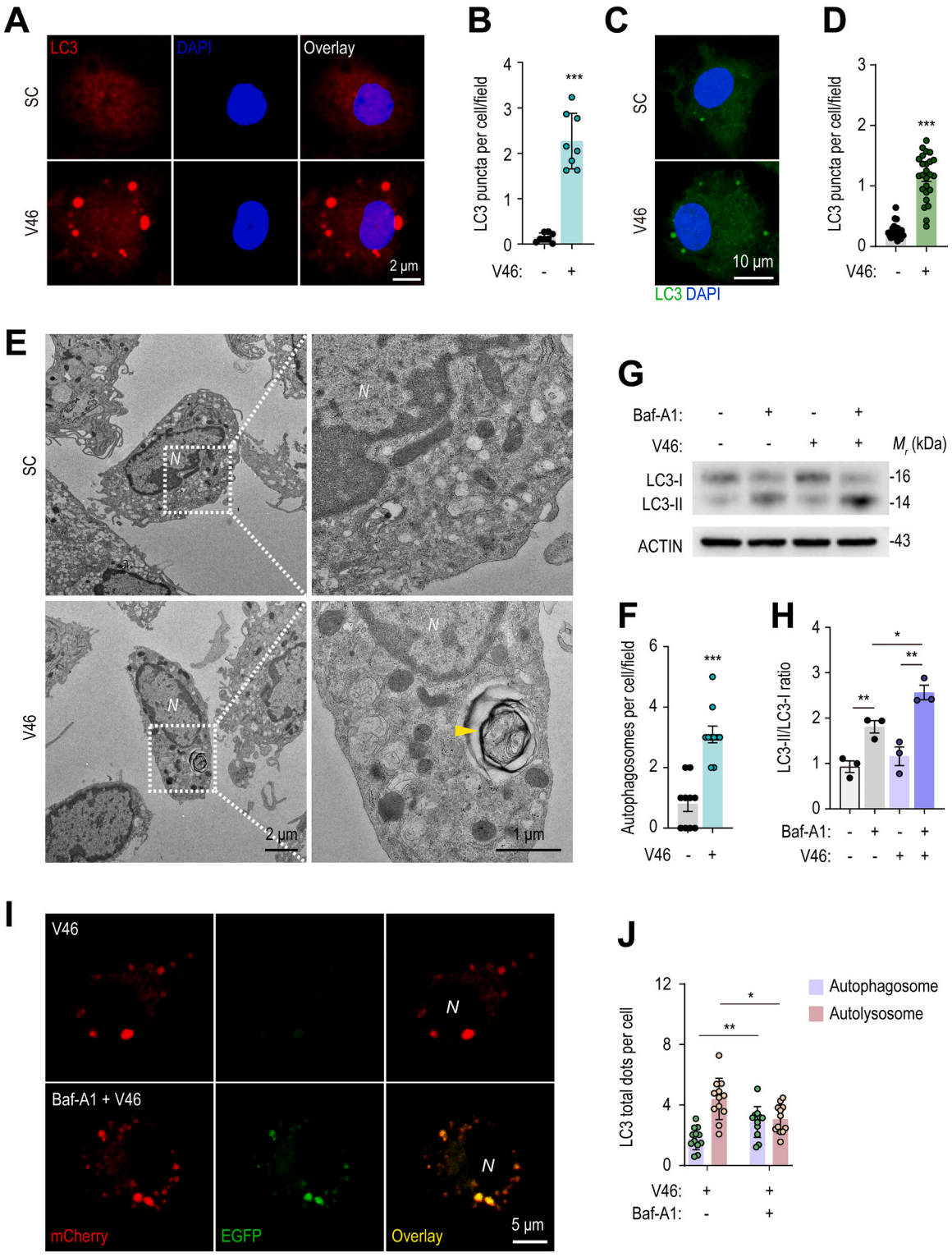

Fig. 5. V46 activates autophagic flux in macrophages. **(A and B)** BMDMs were treated with SC or V46 (100 μM) for 6 h. **(C and D)** hMDMs were treated with SC or V46 (100 μM) for 6 h. **(A-D)** Cells were subjected to confocal microscopy to visualize nuclei or LC3 puncta. **(E and F)** TEM. BMDMs were treated with SC or V46 (100 μM) for 6 h. **(G and H)** BMDMs were pre-treated or not with Baf-A1 (50 nM) for 1 h, followed by treating SC or V46 (20 μM) for 24 h. Cell lysates were subjected to Western blotting using antibodies against LC3-I, LC3-II, and ACTIN. **(I and J)** BMDMs were transduced with retroviruses expressing tandem-tagged mCherry-EGFP-LC3B and incubated for 24 h. Next, cells were pre-incubated with or without Baf-A1 (100 nM) for 2 h, and then followed by treatment with SC or V46 (100 μM) for 24 h. Cells were fixed, permed, and mounted to perform confocal microscopy analysis to assess the puncta with mCherry or EGFP (representing LC3B) per cell. Representative graphs are shown from three independent experiments. We enumerated 50–100 cells in each of over 8 fields per group for quantitative analysis (B, D, and J). Western blot images represent three independent experiments. Band intensities determined by densitometry were normalized to LC3-I (H). Statistical analysis was conducted by two-tailed Student's *t*-test (B, D, F,and H), two-way ANOVA with Sidak's multiple comparison test (J); values represent means ± SDs from three independent experiments. SC, solvent control; Baf-A1, bafilomycin A1; EGFP, enhanced green fluorescent protein; *N*, nucleus; ns, not significant. $*p < 0.05$, $**p < 0.01$, and $***p < 0.001$.

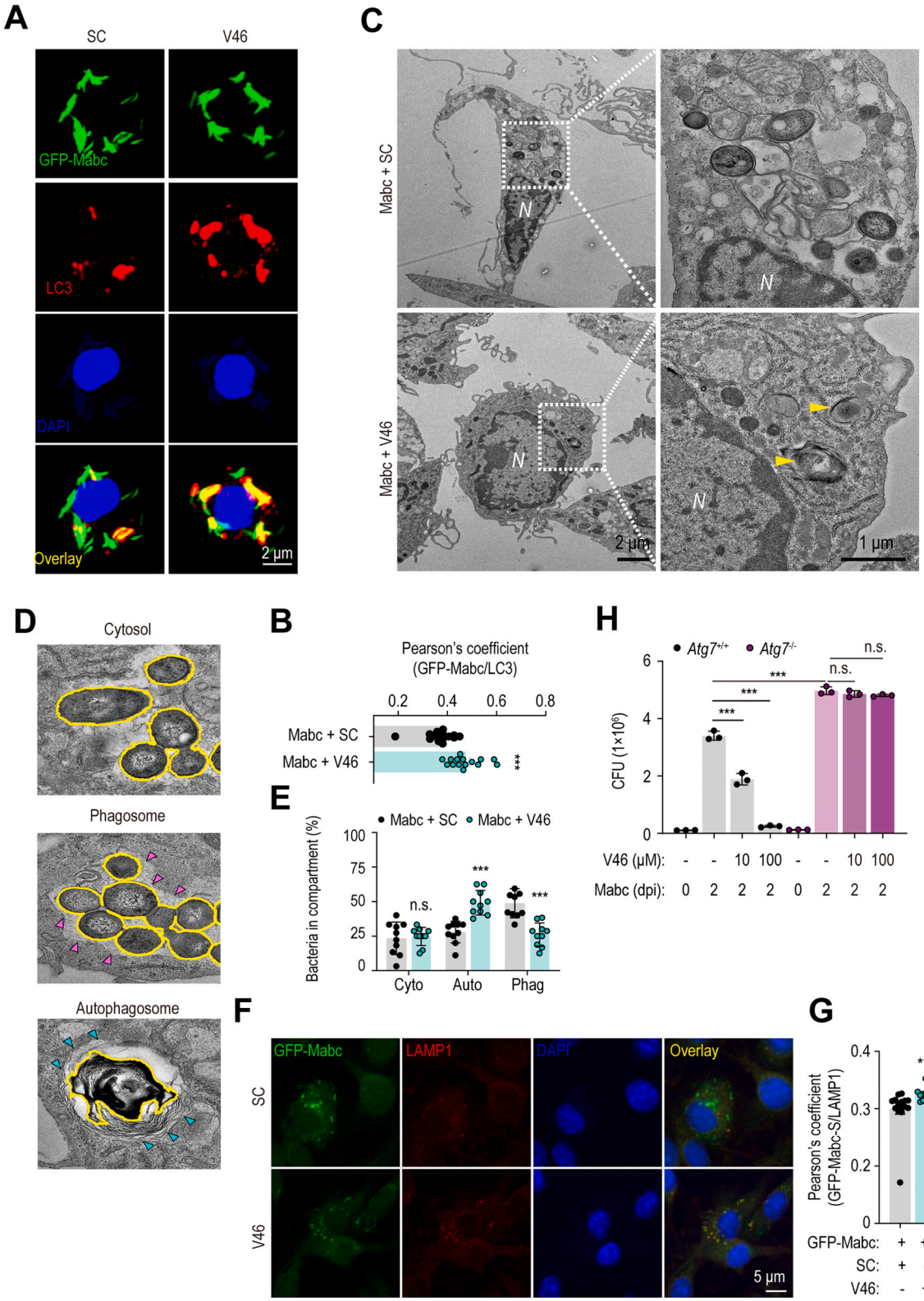

(caption on next page)

Fig. 6. V46 induces autophagic degradation of Mabc in macrophages. **(A and B)** BMDMs were infected with GFP-Mabc (MOI 10) for 2 h, washed twice, and then incubated in the fresh medium containing SC or V46 (100 μM) for 6 h. Representative images (A) and quantitative analysis of intracellular GFP-Mabc colocalization with LC3 (B) are shown. **(C-E)** Mabc-infected (MOI 3) BMDMs were treated with SC or V46 (100 μM) for 6 h. Representative TEM images (C and D) and the ratio of bacteria in each compartments (E) are shown. Yellow circles mean Mabc membranes; magenta arrowheads indicate single host membranes; cyan arrowheads indicate double or multiple host membranes. The percentage of bacteria in compartment within cytosol (24.75 ± 11.17), autophagosome (29.55 ± 7.43), and phagosome (47.72 ± 10.02) from the samples treated with SC and within cytosol (25.00 ± 6.18), autophagosome (48.53 ± 8.43), and phagosome (26.79 ± 7.97) from the samples treated with V46 was counted to conduct quantitative analysis. **(F and G)** GFP-Mabc (MOI 5)-infected BMDMs were treated with SC or V46 (20 μM) for 18 h. Cells were stained with LAMP1 (red) and DAPI (nuclei; blue); representative images (F) and GFP-Mabc colocalization with LAMP1 (G) are shown. **(H)** Bacterial intracellular survival in Mabc-infected (MOI 1) BMDMs from *Atg7* WT and cKO mice treated with SC or V46 (10 or 100 μM) for 2 days. Representative graphs are shown from three independent experiments. We enumerated 50–100 cells in each of over 8 fields per group for quantitative analysis. Statistical analysis was conducted by two-tailed Student's *t*-test (B, E, and G) or one-way ANOVA with Tukey's multiple comparison test (H); values represent means ± SDs from three independent experiments. SC, solvent control; GFP, green fluorescent protein; Mabc, *Mycobacteroides abscessus*; *N*, nucleus; Cyto, cytosol; Auto, autophagosome; Phag, phagosome; CFU, colony-forming unit; dpi, days post-infection; n.s., not significant. $^{***}p < 0.001$.

4. Discussion

The identification of suitable drug candidates to increase host protective immune responses, which are subverted by bacterial pathogens, is a key treatment barrier in Mabc infection. Host defenses can be promoted by modulating inflammation and activating phagosomal maturation and autophagy, thereby eliminating intracellular mycobacteria [12,58]. In this study, V46 showed potential as a host-directed adjunctive therapy against Mabc infection based on its potent effects on autophagy and TFEB activation in both human and murine models. V46, structurally distinct from RSV, has a methoxy group substitution in the benzene ring, resulting in *O*-methylation (Fig. 1A and S1). This type of modification enhances the pharmacological and biochemical properties of compounds, including metabolic stability, membrane transport, and bioavailability [59,60]. Consequently, V46 is expected to have a longer half-life and greater bioavailability compared with RSV, making it a promising candidate drug.

Our findings demonstrate that V46 activates autophagy to enhance antimicrobial responses against Mabc infection. Mechanistic analysis revealed that V46 regulates a key signaling pathway by activating AMPK and suppressing mTOR during Mabc infection. AMPK, a critical metabolic sensor involved in energy balance [61], induces catabolic processes for ATP generation and is associated with mTOR suppression, leading to immunometabolic remodeling and autophagy activation during infection [62,63]. Additionally, V46 significantly induced intracellular Ca^{2+} influx, an upstream signaling event for AMPK activation during Mabc infection. These findings are consistent with a report that phenylbutyrate-mediated autophagy activation and intracellular restriction of Mtb are dependent on intracellular Ca^{2+} influx and subsequent AMPK pathway activation [64]. Additionally, the calcium modulator, flunarizine, enhances intracellular bactericidal effects against Mtb by activating Ca^{2+}/calmodulin-dependent protein kinase II [65]. Considering that the modulation of intracellular Ca^{2+} influx promotes intracellular parasitism by Mtb through inhibition of phagosomal maturation and acidification [65,66], our data suggest that early V46-induced intracellular events related to Ca^{2+} levels are required to suppress the intracellular survival of Mabc. Moreover, V46-mediated antimicrobial responses depend on TFEB, a member of the basic helix-loop-helix-leucine zipper transcription factor family involved in lysosomal biogenesis and autophagy induction [67,68]. TFEB expression and nuclear translocation correlate with the expression levels of and puncta formation by lysosome-related proteins [69]. Indeed, TFEB plays a key role in antimicrobial host defenses against intracellular bacterial infections [18,70,71]. Therefore, V46 can improve lysosomal biogenesis and functions, enhancing antimicrobial responses to Mabc infection.

Upon mycobacterial infection, innate immune defenses are regulated by complex intracellular signaling pathways involving NF-κB, MAPKs, and AKT, which are circumvented or modulated by bacterial virulence factors [72–74]. The ability of V46 to inhibit proinflammatory cytokine/chemokine generation is presumably mediated by its impairment of AKT signaling, considering that V46 reduced AKT phosphorylation in BMDMs during Mabc infection. Although the function of AKT in NTM infection is unclear, its activation of the AKT pathway is associated with enhanced mycobacterial survival in Mtb-infected host cells [75,76]. Therefore, we speculated that V46-induced suppression of AKT enhances host defenses by activating apoptosis. However, V46 was not cytotoxic in BMDMs until 48 h after infection. Alternatively, V46-mediated AKT inhibition may enhance host defenses by promoting autophagy during Mabc infection. Indeed, the protective effects of nilotinib, a tyrosine-kinase inhibitor, against *M. bovis* and *M. avium* subspecies *paratuberculosis* depend on the induction of antibacterial autophagy via phosphoinositide 3-kinase/AKT/mTOR axis suppression by the Abelson tyrosine kinase [77]. Additionally, Mtb protein kinase G inhibits AKT phosphorylation, leading to autophagy induction but not autophagic flux activation [78]. In bluetongue virus infection, AKT pathway suppression is associated with mTOR inactivation, leading to autophagy induction [79]. Taken together, these findings suggest that V46-mediated AKT suppression enhances host defenses against Mabc infection by activating autophagy. Currently, our data showing colocalization of Mabc and LC3 do not identify any specific bacterial effector associated with LC3-positive autophagosomes. Future studies are warranted to clarify which specific Mabc effector or receptor is targeted to LC3-positive autophagosomes in host cells.

Although V46 does not depend on SIRT1 and SIRT3, it significantly inhibits Mabc-mediated inflammation. Inflammatory cytokines and chemokines are upregulated in PBMCs from Mabc-infected patients compared with healthy controls [28]. Both IL-6 and IL-1β promote T helper 17 cell responses; exaggerated forms of these responses are associated with increased neutrophil infiltration and immunopathological responses in patients with active tuberculosis [80]. Mabc-R induces hyperactivation of IL-1β production in macrophages via cytosolic release of oxidized mitochondrial DNA, enhancing intracellular pathogen growth [81]. Furthermore, regulated production of the neutrophil chemokine CXCL2 is important for optimal antimicrobial response during infection, as dysregulation of neutrophil functions is pathogenic in numerous inflammatory disorders [82]. V46 inhibits proinflammatory cytokine and chemokine expression, suggesting that its promotion of host defenses is at least partly mediated by the modulation of pathological inflammation in Mabc infection.

The ZF model enables investigation of the pathogenesis and treatment of Mabc infection. The transparency of ZF larvae facilitates *in vivo* efficacy assessment before progressing to higher organisms [19]. V46 exerted a therapeutic effect in the ZF model by inducing autophagic host defenses against Mabc infection. Furthermore, the activity of V46 was significantly enhanced when combined with RFB. Similarly, the cyclic peptide ohmyungsamycin exerted a synergistic effect with RFB in a ZF model of Mabc infection [26]. RFB, which has potent anti-Mabc activity, exhibits oral bioavailability, extended half-life, and cellular penetration [83,84]. Therefore, the combination of V46 and RFB may be useful in the treatment of Mabc-induced lung disease. However, V46 in combination with CQ resulted in an increased bacterial load, reducing the survival of Mabc-infected ZF. CQ, an autophagy inhibitor, hinders autophagosome–lysosome fusion and slows lysosomal acidification [85]. Thus, V46 inhibits bacterial growth *in vivo* through a mechanism

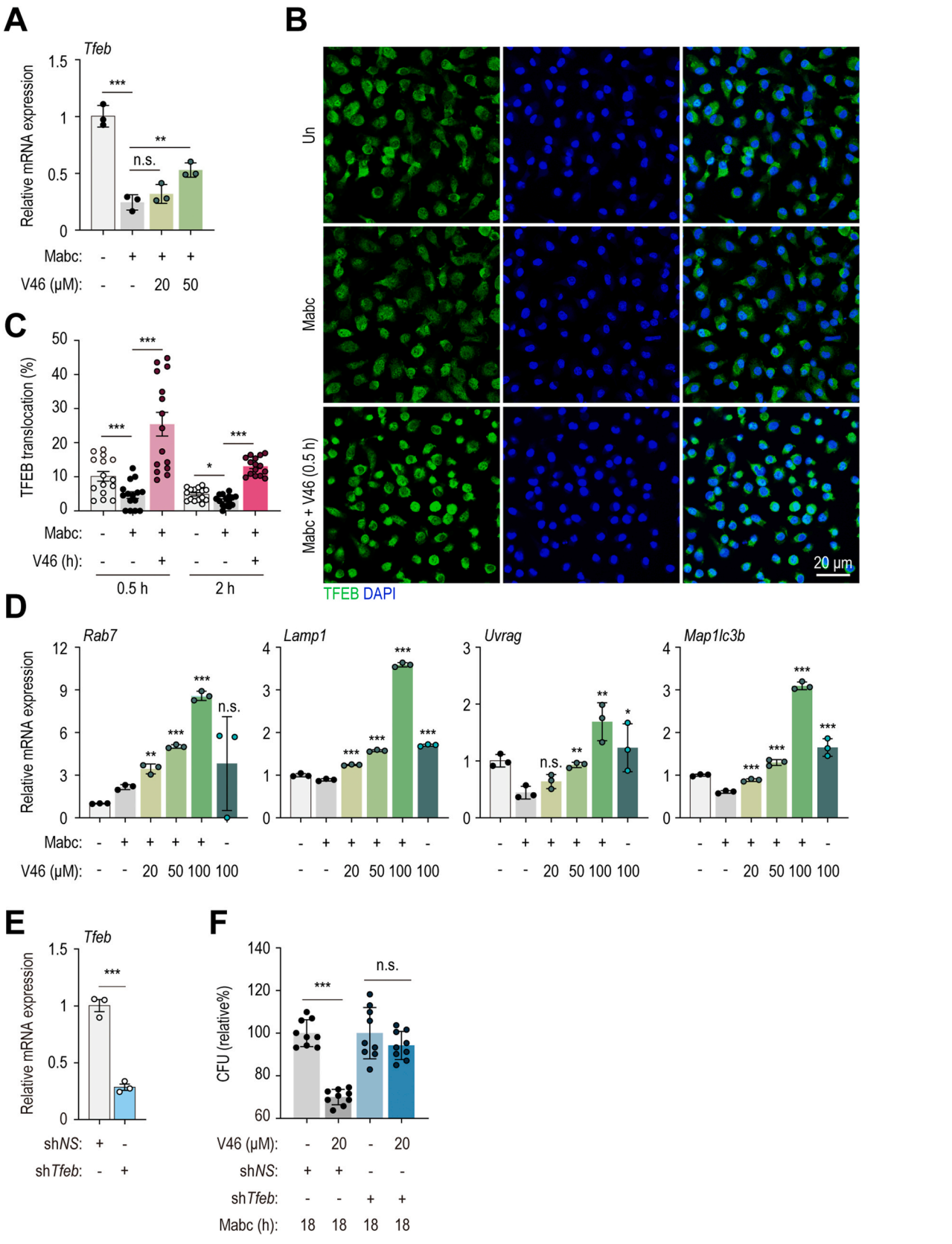

(caption on next page)

Fig. 7. V46 increases TFEB nuclear translocation-mediated activation of autophagy and lysosomal biogenesis in Mabc-infected macrophages. **(A** and **D)** BMDMs were infected with Mabc (MOI 3) or left uninfected for 2 h, then cultured in fresh medium with SC or increasing concentrations (20, 50, or 100 μM) of V46. Cells were collected at 6 h post-treatment and subjected to qRT-PCR of *Tfeb*, *Rab7*, *Lamp1*, *Uvrag*, and *Map1lc3b*. **(B** and **C)** Mabc (MOI 3)-infected or -uninfected BMDMs were treated with SC or V46 (20 μM) for 0.5 or 2 h and harvested. Cells were stained with anti-TFEB (green) and DAPI (nuclei; blue). We enumerated 50 cells in each of 15 fields from three experiments. **(E** and **F)** BMDMs were transduced with lentivirus expressing sh*NS* or sh*Tfeb* for 30 h and infected with Mabc (MOI 1) for 2 h, then cultured in fresh medium with V46 (20 μM) or SC for 18 h. **(E)** Transduction efficiency was verified by qPCR of *Tfeb* expression. **(F)** Intracellular bacterial growth was analyzed by colony counting at 18 h post-infection. Statistical analysis was performed by two-tailed Student's *t*-test (A, D, and E) and one-way ANOVA with Tukey's multiple comparison test (C and F). Error bars denote means ± SDs. Representative graphs and images from three independent experiments are shown. The two-tailed Student's *t*-test conducted in (D) was performed by normalization to SC. Mabc, *Mycobacteroides abscessus*; un, uninfected and untreated; CFU, colony-forming unit; *NS*, nonspecific; n.s., not significant. $*p < 0.05$; $**p < 0.01$, and $***p < 0.001$.

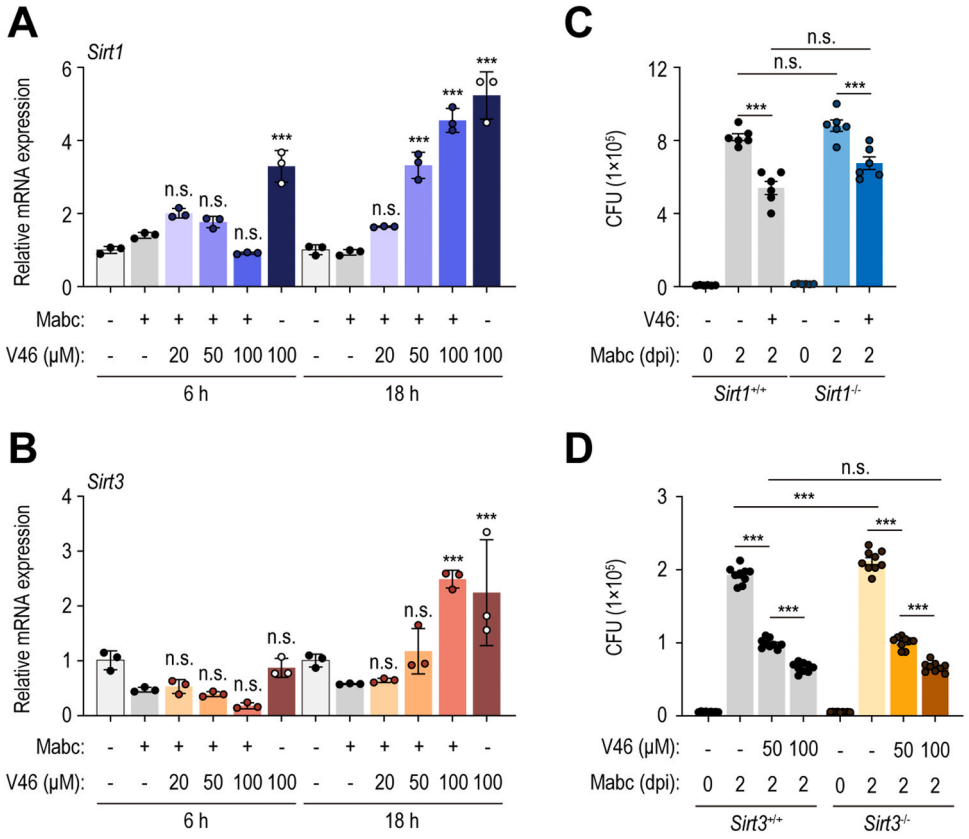

Fig. 8. The antimicrobial activity of V46 is independent of SIRT1- and SIRT3-mediated pathways. **(A** and **B)** BMDMs were infected with Mabc (MOI 3) or left uninfected for 2 h and treated with SC or V46 (20, 50, or 100 μM). Cells were harvested at 6 and 18 h post-treatment, then subjected to qRT-PCR analyses to determine the expression levels of *Sirt1* (A) and *Sirt3* (B). Representative data are shown from three independent experiments. **(C** and **D)** Bacterial intracellular survival in Mabc-infected (MOI 1) BMDMs from *Sirt1* WT/KO **(C)** or *Sirt3* WT/KO **(D)** mice treated with SC or V46 (20 μM in **C**; 50 or 100 μM in **D**). Lysed cells were diluted and spotted on 7H10 medium, and colonies were enumerated after 3 days of incubation. Data are from three independent experiments. Statistical significance was determined by one-way ANOVA with Tukey's multiple comparison test (A-D). Error bars denote means ± SDs. Mabc, *Mycobacteroides abscessus*; CFU, colony-forming unit; dpi, days post-infection; ns, not significant. $***p < 0.001$.

involving autophagy and lysosomal pathways.

5. Conclusion

Overall, our findings suggest that V46 has potential as an adjunctive therapy that enhances autophagy to strengthen innate host defenses against Mabc infection. Mechanistic analysis showed that V46 activates Ca^{2+}-AMPK-mediated autophagy and TFEB signaling, thereby restricting the intracellular survival of Mabc. V46 has a longer half-life and greater bioavailability compared with RSV, enhancing its therapeutic potential. V46 can attenuate MDR-Mabc infection *in vivo*, making it valuable for efforts to combat resistant strains. The V46-RFB combination exerted a synergistic bactericidal effect against Mabc, suggesting that it can enhance therapeutic outcomes. Therefore, V46 is a promising candidate for host-directed therapies targeting Mabc infection.

Ethics approval statement

The mice study was reviewed and approved by the Institutional Animal Care and Use Committee (202109A-CNU-180; South Korea) and the Institutional Research and Ethics Committee (201912A-CNU-203; Daejeon Korea) of Chungnam National University College of Medicine. All ZF experiments were approved by the Animal Research Ethics Committee of Gyeongsang National University (Project identification code: GNU-220710-E0078, Approval date: 10 Jul 2022). The data with human samples (healthy volunteers) were obtained from approval of an ongoing Institutional Review Board. This study was confirmed by the Institutional Research and Ethics Committee at Chungnam National University Hospital (CNUH 2023–05–034–005; Daejeon, Korea).

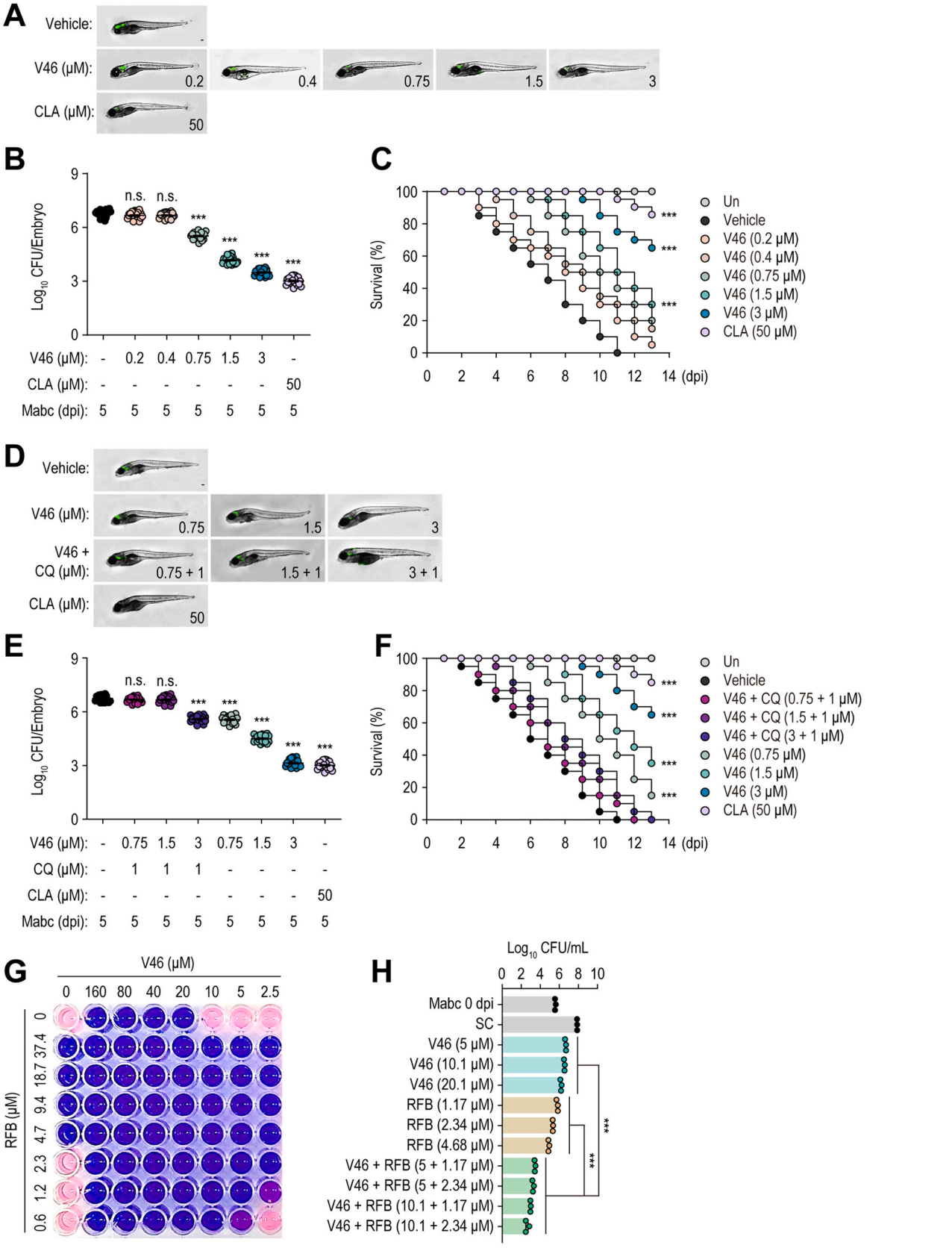

(caption on next page)

Fig. 9. The *in vivo* efficacy of V46 is autophagy-dependent in the ZF model and shows synergistic effects with other drugs. **(A)** Evaluation of *in vivo* V46 activity using GFP-Mabc infection. GFP-Mabc was injected via the caudal vein and visualized in vehicle-, V46 (0.2, 0.4, 0.75, 1,5, or 3 μM), or CLA (50 μM)-treated embryos by fluorescence microscopy. **(B)** Bacterial burden in vehicle-, V46 (0.2, 0.4, 0.75, 1,5, or 3 μM)- and CLA (50 μM)-treated ZF at 5 dpi. **(C)** Survival curve of GFP-Mabc-infected embryos treated with V46 (n = 20, representative of three independent experiments). **(D)** *In vivo* evaluation of vehicle, CLA, and V46 alone and in combination with CQ. ZF were infected with GFP-Mabc and treated with vehicle, CLA (50 μM), or V46 (0.75, 1.5, or 3 μM) or co-treated with V46 (0.75, 1.5, and 3 μM) and CQ (1 μM). **(E)** Bacterial burdens of ZF treated with vehicle, CLA, V46 alone, and V46 plus CQ, expressed as mean $\log_{10}$ CFUs per embryo (n = 20 for each condition) from three independent experiments. **(F)** Survival curves of Mabc-infected embryos treated with vehicle, CLA (50 μM), V46 (0.75, 1.5, and 3 μM) or co-treated with V46 and CQ (1 μM). **(G)** Drug interactions were evaluated by checkerboard assay using V46 (horizontal) in combination with RFB (vertical). Mabc was grown in medium containing V46 alone or in combination with RFB. **(H)** Live bacteria were enumerated on 7H10 agar. Mabc was grown in medium containing V46 alone or in combination with RFB. Error bars denote means ± SDs from three independent experiments. One-way ANOVA with Tukey's multiple comparison (**B**, **E** [difference compared with vehicle control] and **H**) and log-rank (Mantel—Cox) tests (**C** and **F**) were used to determine statistical significance. CLA, clarithromycin; CFU, colony-forming unit; Mabc, *Mycobacteroides abscessus*; dpi, days post-infection; CQ, chloroquine diphosphate salt; ns, not significant. SC, solvent control; RFB, rifabutin. ***$p < 0.001$.

Table 1
MIC_{50} values of anti-Mabc drugs against Mabc and interaction profiles with V46 evaluated by REMA checkerboard assay.

Assigned name	MIC_{50} (μM) by REMA	Interaction profile with V46	
		ΣFIC	Outcome
V46	20.12		
CLA	4.95	1.23	Additive
OMD	1.71	1.33	Additive
AMK	11.10	1.31	Additive
RFB	4.68	0.46	Synergistic
IMP	3.6	1.35	Additive
BDQ	0.58	1.35	Additive
CFX	0.23	1.32	Additive

MIC_{50}, MIC required to suppress bacterial growth by 50 %; FIC, fractional inhibitory concentration; CLA, clarithromycin; OMD, omadacycline; AMK, amikacin; RFB, rifabutin; IMP, imipenem; BDQ, bedaquiline; CFX, cefoxitin

Funding statement

This work was supported by the National Research Foundation (NRF) of Korea grant funded by the Korea government (MSIT) (No. RS-2023-00255021) at Chungnam National University, (No. 2020R1A2C1004077) at Gyeongsang National University, and (No. 2022M3H9A2083956 to H.S.K.) at the Korea Basic Science Institute. This research was also supported by Basic Science Research program through NRF of Korea funded by the Ministry of Education (No. RS-2023-00249417) at Chungnam National university. Additionally, this research was supported by the Korea Basic Science Institute under the R&D program (Project No. C330430) supervised by the Ministry of Science and ICT. This research was further supported by a grant of the Korea Health Technology R&D Project through the Korea Health Industry Development Institute (KHIDI), funded by the Ministry of Health & Welfare, Republic of Korea (No. HI22C1361). The author of this paper (Asmita Sapkota) is a Global Korea Scholarship scholar sponsored by the Korean Government.

CRediT authorship contribution statement

Asmita Sapkota: Writing – original draft, Validation, Investigation, Formal analysis. **Eun-Jin Park:** Writing – review & editing, Writing – original draft, Validation, Investigation, Formal analysis, Data curation. **Young Jae Kim:** Writing – original draft, Validation, Methodology, Investigation, Formal analysis, Data curation, Writing – review & editing. **Jong Beom Heo:** Writing – original draft, Validation, Resources, Investigation, Data curation. **Thanh Quang Nguyen:** Validation, Investigation, Formal analysis. **Bo Eun Heo:** Investigation, Formal analysis. **Jin Kyung Kim:** Validation, Investigation, Formal analysis. **Sang-Hee Lee:** Investigation, Data curation. **Soo In Kim:** Validation, Investigation. **Yoon-Jung Choi:** Resources, Investigation. **Taylor Roh:** Formal analysis, Data curation. **Sang Min Jeon:** Validation, Resources, Investigation, Formal analysis. **Marnpyung Jang:** Investigation. **Hae Joon Heo:** Resources. **Jake Whang:** Resources. **Seungwha Paik:** Validation, Investigation, Formal analysis, Data curation. **Jae-Min Yuk:** Resources. **Jin-Man Kim:** Formal analysis. **Gyu Yong Song:** Supervision, Resources, Methodology, Data curation. **Jichan Jang:** Writing – original draft, Supervision, Methodology, Funding acquisition, Data curation. **Eun-Kyeong Jo:** Writing – review & editing, Writing – original draft, Supervision, Resources, Project administration, Methodology, Funding acquisition, Data curation, Conceptualization.

Declaration of Competing Interest

All authors declare that they have no known competing financial interests or relationships that could have appeared to influence the work reported in this paper.

Data Availability

Data will be made available on request.

Acknowledgements

We thank Dr. Laurent Kremer (CNRS, IRIM, Université de Montpellier, Montpellier, France) for kind provision of Mabc-S ($CIP104536^T$) and -R ($CIP104536^T$); Prof. Hyun Seok Kim (Ehwa Womans University, Seoul, Korea) for the kind provision of *Sirt3* KO mice; Prof. Byung-Hun Park (Chonbuk National University, Jeonju, Korea) for the kind provision of *Sirt1* KO mice. Prof. Masaaki Komatsu for kind provision of *Atg7*-floxed mice. We thank Dr. H.W. Suh and Ms. S.G. Shin for their excellent technical assistance. To current and past members of our Medical Research Center (*i*-MRC), we are always grateful for the investigations and discussions that contributed to this article.

Appendix A. Supporting information

Supplementary data associated with this article can be found in the online version at doi:10.1016/j.biopha.2024.117313.

References

[1] M.D. Johansen, J.L. Herrmann, L. Kremer, Non-tuberculous mycobacteria and the rise of *Mycobacterium abscessus*, Nat. Rev. Microbiol. 18 (2020) 392–407.
[2] G. Degiacomi, J.C. Sammartino, L.R. Chiarelli, O. Riabova, V. Makarov, M.R. Pasca, *Mycobacterium abscessus,* an emerging and worrisome pathogen among cystic fibrosis patients, Int. J. Mol. Sci. 20 (2019) 5868.
[3] K. Bachar, T. Shulimzon, M.J. Segel, Nontuberculous mycobacteria infections of the pleura: a systematic review, Respir. Med 205 (2022) 107036.
[4] I. Shah, F. Shah, Nontuberculous mycobacterial empyema in an immunocompetent child, Indian J. Pathol. Microbiol. 61 (2018) 141–142.
[5] E. Tortoli, T.A. Kohl, B.A. Brown-Elliott, A. Trovato, S.C. Leao, M.J. Garcia, et al., Emended description of *Mycobacterium abscessus*, *Mycobacterium abscessus* subsp. *abscessus* and *Mycobacterium abscessus* subsp. *bolletii* and designation of *Mycobacterium abscessus* subsp. *massiliense* comb. nov, Int. J. Syst. Evol. Microbiol. 66 (2016) 4471–4479.
[6] D.E. Griffith, B.A. Brown-Elliott, J.L. Benwill, R.J. Wallace Jr., *Mycobacterium abscessus.* "Pleased to meet you, hope you guess my name…", Ann. Am. Thorac. Soc. 12 (2015) 436–439.
[7] M. Meir, D. Barkan, Alternative and experimental therapies of *Mycobacterium abscessus* infections, Int. J. Mol. Sci. 21 (2020) 6793.

[8] K. To, R. Cao, A. Yegiazaryan, J. Owens, V. Venketaraman, General overview of nontuberculous mycobacteria opportunistic pathogens: *Mycobacterium avium* and *Mycobacterium abscessus*, J. Clin. Med. 9 (2020) 2541.

[9] J.Y. Kam, E. Hortle, E. Krogman, S.E. Warner, K. Wright, K. Luo, et al., Rough and smooth variants of *Mycobacterium abscessus* are differentially controlled by host immunity during chronic infection of adult zebrafish, Nat. Commun. 13 (2022) 952.

[10] S.L. Baltierra-Uribe, Mde J. Garcia-Vasquez, N.S. Castrejon-Jimenez, M.P. Estrella-Pinon, J. Luna-Herrera, B.E. Garcia-Perez, Mycobacteria entry and trafficking into endothelial cells, Can. J. Microbiol. 60 (2014) 569–577.

[11] E.J. Strong, S. Lee, Targeting autophagy as a strategy for developing new vaccines and host-directed therapeutics against mycobacteria, Front Microbiol. 11 (2020) 614313.

[12] M. Shamaei, M. Mirsaeidi, Nontuberculous mycobacteria, macrophages, and host innate immune response, Infect. Immun. 89 (2021) e0081220.

[13] M. Renna, C. Schaffner, K. Brown, S. Shang, M.H. Tamayo, K. Hegyi, et al., Azithromycin blocks autophagy and may predispose cystic fibrosis patients to mycobacterial infection, J. Clin. Invest. 121 (2011) 3554–3563.

[14] Y.S. Kim, J.K. Kim, B.T.B. Hanh, S.Y. Kim, H.J. Kim, Y.J. Kim, et al., The peroxisome proliferator-activated receptor alpha-agonist gemfibrozil promotes defense against *Mycobacterium abscessus* infections, Cells 9 (2020) 648.

[15] C.R. Park, S. Paik, Y.J. Kim, J.K. Kim, S.M. Jeon, S.H. Lee, et al., Rufomycin exhibits dual effects against *Mycobacterium abscessus* infection by inducing host defense and antimicrobial activities, Front Microbiol. 12 (2021) 695024.

[16] K. Sachdeva, V. Sundaramurthy, The interplay of host lysosomes and intracellular pathogens, Front Cell Infect. Microbiol. 10 (2020) 595502.

[17] V. Ammanathan, P. Mishra, A.K. Chavalmane, S. Muthusamy, V. Jadhav, C. Siddamadappa, et al., Restriction of intracellular Salmonella replication by restoring TFEB-mediated xenophagy, Autophagy 16 (2020) 1584–1597.

[18] E.M. Schuster, M.W. Epple, K.M. Glaser, M. Mihlan, K. Lucht, J.A. Zimmermann, et al., TFEB induces mitochondrial itaconate synthesis to suppress bacterial growth in macrophages, Nat. Metab. 4 (2022) 856–866.

[19] T.H. Kim, B.T.B. Hanh, G. Kim, D.G. Lee, J.W. Park, S.E. Lee, et al., Thiostrepton: a novel therapeutic drug candidate for *Mycobacterium abscessus* infection, Molecules 24 (2019) 4511.

[20] N. Pannu, A. Bhatnagar, Resveratrol: from enhanced biosynthesis and bioavailability to multitargeting chronic diseases, Biomed. Pharm. 109 (2019) 2237–2251.

[21] F. Sparvoli, C. Martin, A. Scienza, G. Gavazzi, C. Tonelli, Cloning and molecular analysis of structural genes involved in flavonoid and stilbene biosynthesis in grape (Vitis vinifera L.), Plant Mol. Biol. 24 (1994) 743–755.

[22] T. Szkudelski, K. Szkudelska, Anti-diabetic effects of resveratrol, Ann. N. Y Acad. Sci. 1215 (2011) 34–39.

[23] G. Chhabra, C.K. Singh, D. Amiri, N. Akula, N. Ahmad, Recent advancements on immunomodulatory mechanisms of resveratrol in tumor microenvironment, Molecules 26 (2021).

[24] T. Walle, F. Hsieh, M.H. DeLegge, J.E. Oatis Jr., U.K. Walle, High absorption but very low bioavailability of oral resveratrol in humans, Drug Metab. Dispos. 32 (2004) 1377–1382.

[25] J.K. Kim, Y.S. Kim, H.M. Lee, H.S. Jin, C. Neupane, S. Kim, et al., GABAergic signaling linked to autophagy enhances host protection against intracellular bacterial infections, Nat. Commun. 9 (2018) 4184.

[26] S.M. Jeon, Y.J. Kim, T.Q. Nguyen, J. Cui, B. Thi Bich Hanh, P. Silwal, et al., Ohmyungsamycin promotes M1-like inflammatory responses to enhance host defence against *Mycobacteroides abscessus* infections, Virulence 13 (2022) 1966–1984.

[27] A. Bernut, C. Dupont, A. Sahuquet, J.L. Herrmann, G. Lutfalla, L. Kremer, Deciphering and imaging pathogenesis and cording of *Mycobacterium abscessus* in zebrafish embryos, J. Vis. Exp. (2015), https://doi.org/10.3791/5313053130.

[28] H.J. Kim, I.S. Kim, S.G. Lee, Y.J. Kim, P. Silwal, J.Y. Kim, et al., MiR-144-3p is associated with pathological inflammation in patients infected with *Mycobacteroides abscessus*, Exp. Mol. Med. 53 (2021) 136–149.

[29] J.K. Kim, Y.S. Kim, H.M. Lee, H.S. Jin, C. Neupane, S. Kim, et al., GABAergic signaling linked to autophagy enhances host protection against intracellular bacterial infections, Nat. Commun. 9 (2018) 4184.

[30] E.L. Benard, A.M. van der Sar, F. Ellett, G.J. Lieschke, H.P. Spaink, A.H. Meijer, Infection of zebrafish embryos with intracellular bacterial pathogens, J. Vis. Exp. (2012), https://doi.org/10.3791/37813781.

[31] T.Q. Nguyen, B.E. Heo, B.T.B. Hanh, S. Jeon, Y. Park, A. Choudhary, et al., DS86760016, a Leucyl-tRNA synthetase inhibitor, is active against *Mycobacterium abscessus*, Antimicrob. Agents Chemother. 67 (2023) e0156722.

[32] B.T. Bich Hanh, N.T. Quang, Y. Park, B.E. Heo, S. Jeon, J.W. Park, et al., Omadacycline potentiates clarithromycin activity against *Mycobacterium abscessus*, Front Pharm. 12 (2021) 790767.

[33] T.Q. Nguyen, B.T.B. Hanh, S. Jeon, B.E. Heo, Y. Park, A. Choudhary, et al., Synergistic effect of Q203 combined with PBTZ169 against *Mycobacterium tuberculosis*, Antimicrob. Agents Chemother. 66 (2022) e0044822.

[34] E. Story-Roller, E.C. Maggioncalda, G. Lamichhane, Select beta-lactam combinations exhibit synergy against *Mycobacterium abscessus in vitro*, Antimicrob. Agents Chemother. 63 (2019) e02613-18.

[35] V. Le Moigne, C. Raynaud, F. Moreau, C. Dupont, J. Nigou, O. Neyrolles, et al., Efficacy of bedaquiline, alone or in combination with imipenem, against *Mycobacterium abscessus* in C3HeB/FeJ mice, Antimicrob. Agents Chemother. 64 (2020) e00114. -20.

[36] K.C. Ferrell, M.D. Johansen, J.A. Triccas, C. Counoupas, Virulence mechanisms of *Mycobacterium abscessus*: current knowledge and implications for vaccine design, Front Microbiol. 13 (2022) 842017.

[37] C.B. Ching, S. Gupta, B. Li, H. Cortado, N. Mayne, A.R. Jackson, et al., Interleukin-6/Stat3 signaling has an essential role in the host antimicrobial response to urinary tract infection, Kidney Int. 93 (2018) 1320–1329.

[38] Y.J. Kim, E.J. Park, S.H. Lee, P. Silwal, J.K. Kim, J.S. Yang, et al., Dimethyl itaconate is effective in host-directed antimicrobial responses against mycobacterial infections through multifaceted innate immune pathways, Cell Biosci. 13 (2023) 49.

[39] G. Kilinc, A. Saris, T.H.M. Ottenhoff, M.C. Haks, Host-directed therapy to combat mycobacterial infections, Immunol. Rev. 301 (2021) 62–83.

[40] B.D. Manning, A. Toker, AKT/PKB signaling: navigating the network, Cell 169 (2017) 381–405.

[41] J. Jia, B. Bissa, L. Brecht, L. Allers, S.W. Choi, Y. Gu, et al., AMPK is activated during lysosomal damage via a galectin-ubiquitin signal transduction system, Autophagy 16 (2020) 1550–1552.

[42] Y.M. Chen, P.Y. Liu, K.T. Tang, H.J. Liu, T.L. Liao, TWEAK-Fn14 axis induces calcium-associated autophagy and cell death to control mycobacterial survival in macrophages, Microbiol Spectr. 10 (2022) e0317222.

[43] S. Soni, Y. Jiang, L. Zhang, A. Thakur, S. Cataltepe, AMPK-driven macrophage responses are autophagy dependent in experimental bronchopulmonary dysplasia, Am. J. Respir. Cell Mol. Biol. 68 (2023) 279–287.

[44] W. Liu, J. Zhuang, Y. Jiang, J. Sun, R.A. Prinz, J. Sun, et al., Toll-like receptor signalling cross-activates the autophagic pathway to restrict *Salmonella* Typhimurium growth in macrophages, Cell Microbiol. 21 (2019) e13095.

[45] C. Mauvezin, T.P. Neufeld, Bafilomycin A1 disrupts autophagic flux by inhibiting both V-ATPase-dependent acidification and Ca-P60A/SERCA-dependent autophagosome-lysosome fusion, Autophagy 11 (2015) 1437–1438.

[46] X. Han, Y. Tang, Y. Zhang, J. Zhang, Z. Hu, W. Xu, et al., Impaired V-ATPase leads to increased lysosomal pH, results in disrupted lysosomal degradation and autophagic flux blockage, contributes to fluoride-induced developmental neurotoxicity, Ecotoxicol. Environ. Saf. 236 (2022) 113500.

[47] B. Aylan, E.M. Bernard, E. Pellegrino, L. Botella, A. Fearns, N. Athanasiadi, et al., ATG7 and ATG14 restrict cytosolic and phagosomal *Mycobacterium tuberculosis* replication in human macrophages, Nat. Microbiol. 8 (2023) 803–818.

[48] Q. Chai, X. Wang, L. Qiang, Y. Zhang, P. Ge, Z. Lu, et al., A *Mycobacterium tuberculosis* surface protein recruits ubiquitin to trigger host xenophagy, Nat. Commun. 10 (2019) 1973.

[49] T.R. Lerner, C.J. Queval, A. Fearns, U. Repnik, G. Griffiths, M.G. Gutierrez, Phthiocerol dimycocerosates promote access to the cytosol and intracellular burden of *Mycobacterium tuberculosis* in lymphatic endothelial cells, BMC Biol. 16 (2018) 1.

[50] T.R. Lerner, C. de Souza Carvalho-Wodarz, U. Repnik, M.R. Russell, S. Borel, C. R. Diedrich, et al., Lymphatic endothelial cells are a replicative niche for *Mycobacterium tuberculosis*, J. Clin. Invest. 126 (2016) 1093–1108.

[51] J.A. Martina, Y. Chen, M. Gucek, R. Puertollano, MTORC1 functions as a transcriptional regulator of autophagy by preventing nuclear transport of TFEB, Autophagy 8 (2012) 903–914.

[52] M. Palmieri, R. Pal, M. Sardiello, AKT modulates the autophagy-lysosome pathway via TFEB, Cell Cycle 16 (2017) 1237–1238.

[53] A. Nakashima, S.B. Cheng, M. Ikawa, T. Yoshimori, W.J. Huber, R. Menon, et al., Evidence for lysosomal biogenesis proteome defect and impaired autophagy in preeclampsia, Autophagy 16 (2020) 1771–1785.

[54] Y. Song, C. Quach, C. Liang, UVRAG in autophagy, inflammation, and cancer, Autophagy 16 (2020) 387–388.

[55] D.S. Moraes, D.C. Moreira, J.M.O. Andrade, S.H.S. Santos, Sirtuins, brain and cognition: a review of resveratrol effects, IBRO Rep. 9 (2020) 46–51.

[56] Q. Sun, R.R. Kang, K.G. Chen, K. Liu, Z. Ma, C. Liu, et al., Sirtuin 3 is required for the protective effect of resveratrol on manganese-induced disruption of mitochondrial biogenesis in primary cultured neurons, J. Neurochem. 156 (2021) 121–135.

[57] K.N. Kragh, D. Gijon, A. Maruri, A. Antonelli, M. Coppi, M. Kolpen, et al., Effective antimicrobial combination *in vivo* treatment predicted with microcalorimetry screening, J. Antimicrob. Chemother. 76 (2021) 1001–1009.

[58] M. Bar-Oz, M. Meir, D. Barkan, Virulence-associated secretion in *Mycobacterium abscessus*, Front Immunol. 13 (2022) 938895.

[59] N. Koirala, N.H. Thuan, G.P. Ghimire, D.V. Thang, J.K. Sohng, Methylation of flavonoids: chemical structures, bioactivities, progress and perspectives for biotechnological production, Enzym. Micro Technol. 86 (2016) 103–116.

[60] X. Wen, T. Walle, Methylated flavonoids have greatly improved intestinal absorption and metabolic stability, Drug Metab. Dispos. 34 (2006) 1786–1792.

[61] D. Grahame Hardie, AMP-activated protein kinase: a key regulator of energy balance with many roles in human disease, J. Intern Med. 276 (2014) 543–559.

[62] J. Sanchez-Garrido, A.R. Shenoy, Regulation and repurposing of nutrient sensing and autophagy in innate immunity, Autophagy 17 (2021) 1571–1591.

[63] R. Ganesan, N.J. Hos, S. Gutierrez, J. Fischer, J.M. Stepek, E. Daglidu, et al., *Salmonella* Typhimurium disrupts Sirt1/AMPK checkpoint control of mTOR to impair autophagy, PLoS Pathog. 13 (2017) e1006227.

[64] R.S. Rekha, S.S. Rao Muvva, M. Wan, R. Raqib, P. Bergman, S. Brighenti, et al., Phenylbutyrate induces LL-37-dependent autophagy and intracellular killing of *Mycobacterium tuberculosis* in human macrophages, Autophagy 11 (2015) 1688–1699.

[65] S. Mo, X. Liu, K. Zhang, W. Wang, Y. Cai, Q. Ouyang, et al., Flunarizine suppresses *Mycobacterium tuberculosis* growth via calmodulin-dependent phagosome maturation, J. Leukoc. Biol. 111 (2022) 1021–1029.

[66] Z.A. Malik, S.S. Iyer, D.J. Kusner, *Mycobacterium tuberculosis* phagosomes exhibit altered calmodulin-dependent signal transduction: contribution to inhibition of phagosome-lysosome fusion and intracellular survival in human macrophages, J. Immunol. 166 (2001) 3392–3401.
[67] S. Kim, H.S. Song, J. Yu, Y.M. Kim, MiT family transcriptional factors in immune cell functions, Mol. Cells 44 (2021) 342–355.
[68] R. Curnock, K. Yalci, J. Palmfeldt, M. Jaattela, B. Liu, B. Carroll, TFEB-dependent lysosome biogenesis is required for senescence, EMBO J. 42 (2023) e111241.
[69] S.J. Jeong, J. Stitham, T.D. Evans, X. Zhang, A. Rodriguez-Velez, Y.S. Yeh, et al., Trehalose causes low-grade lysosomal stress to activate TFEB and the autophagy-lysosome biogenesis response, Autophagy 17 (2021) 3740–3752.
[70] R. Dwivedi, P. Baindara, Differential regulation of TFEB-induced autophagy during Mtb infection and starvation, Microorganisms 11 (2023).
[71] S.L. Lu, H. Omori, Y. Zhou, Y.S. Lin, C.C. Liu, J.J. Wu, et al., VEGF-mediated augmentation of autophagic and lysosomal activity in endothelial cells defends against intracellular *Streptococcus pyogenes*, mBio 13 (2022) e0123322.
[72] R. Abreu, P. Giri, F. Quinn, Host-pathogen interaction as a novel target for host-directed therapies in tuberculosis, Front Immunol. 11 (2020) 1553.
[73] Q. Chai, L. Wang, C.H. Liu, B. Ge, New insights into the evasion of host innate immunity by *Mycobacterium tuberculosis*, Cell Mol. Immunol. 17 (2020) 901–913.
[74] M.A. Mir, B. Mir, M. Kumawat, M. Alkhanani, U. Jan, Manipulation and exploitation of host immune system by pathogenic *Mycobacterium tuberculosis* for its advantage, Future Microbiol. 17 (2022) 1171–1198.
[75] S. Lochab, Y. Singh, S. Sengupta, V.K. Nandicoori, *Mycobacterium tuberculosis* exploits host ATM kinase for survival advantage through SecA2 secretome, Elife 9 (2020) e51466.
[76] C. Kuijl, N.D. Savage, M. Marsman, A.W. Tuin, L. Janssen, D.A. Egan, et al., Intracellular bacterial growth is controlled by a kinase network around PKB/AKT1, Nature 450 (2007) 725–730.
[77] T. Hussain, D. Zhao, S.Z.A. Shah, N. Sabir, J. Wang, Y. Liao, et al., Nilotinib: A tyrosine kinase inhibitor mediates resistance to intracellular mycobacterium via regulating autophagy, Cells 8 (2019) 506.
[78] P. Ge, Z. Lei, Y. Yu, Z. Lu, L. Qiang, Q. Chai, et al., *M. tuberculosis* PknG manipulates host autophagy flux to promote pathogen intracellular survival, Autophagy 18 (2022) 576–594.
[79] S. Lv, Q.Y. Xu, E.C. Sun, J.K. Zhang, D.L. Wu, Dissection and integration of the autophagy signaling network initiated by bluetongue virus infection: crucial candidates ERK1/2, Akt and AMPK, Sci. Rep. 6 (2016) 23130.
[80] G. Pollara, C.T. Turner, J. Rosenheim, A. Chandran, L.C.K. Bell, A. Khan, et al., Exaggerated IL-17A activity in human *in vivo* recall responses discriminates active tuberculosis from latent infection and cured disease, Sci. Transl. Med. 13 (2021) eabg7673.
[81] B.R. Kim, B.J. Kim, Y.H. Kook, B.J. Kim, *Mycobacterium abscessus* infection leads to enhanced production of type 1 interferon and NLRP3 inflammasome activation in murine macrophages via mitochondrial oxidative stress, PLoS Pathog. 16 (2020) e1008294.
[82] K. Rajarathnam, M. Schnoor, R.M. Richardson, S. Rajagopal, How do chemokines navigate neutrophils to the target site: Dissecting the structural mechanisms and signaling pathways, Cell Signal 54 (2019) 69–80.
[83] D.B. Aziz, J.L. Low, M.L. Wu, M. Gengenbacher, J.W.P. Teo, V. Dartois, et al., Rifabutin is active against *Mycobacterium abscessus* complex, Antimicrob. Agents Chemother. 61 (2017).
[84] J. Chen, H. Zhang, Q. Guo, S. He, L. Xu, Z. Zhang, et al., *In vitro* activity of rifabutin against *Mycobacterium abscessus*, clinical isolates, Clin. Exp. Pharm. Physiol. 49 (2022) 767–775.
[85] H. Ye, M. Chen, F. Cao, H. Huang, R. Zhan, X. Zheng, Chloroquine, an autophagy inhibitor, potentiates the radiosensitivity of glioma initiating cells by inhibiting autophagy and activating apoptosis, BMC Neurol. 16 (2016) 178.